OSMIUM MASS BALANCE IN PERIDOTITE AND THE EFFECTS OF MANTLE-DERIVED SULFIDES ON BASALT PETROGENESIS

J. Harvey[1,2*], C.W. Dale[3], A. Gannoun[1,4], K.W. Burton, [1,3,5]

[1] Dept. of Earth & Environmental Sciences, The Open University, Milton Keynes, UK.

[2] Current address, School of Earth & Environment, University of Leeds, UK.

[3] Dept. of Earth Sciences, Durham University, UK.

[4] Laboratoire des Magmas et Volcans, Université Blaise Pascal, Clermont-Ferrand, France.

[5] Dept. of Earth Sciences, University of Oxford, UK.

* Corresponding author: email *j.harvey@open.ac.uk* / *feejh@leeds.ac.uk*

ABSTRACT

Analyses of enriched mantle (EM)-basalts, using lithophile element-based isotope systems, have long provided evidence for discrete mantle reservoirs with variable composition. Upon partial melting, the mantle reservoir imparts its isotopic fingerprint upon the partial melt produced. However, it has increasingly been recognised that it may not be simple to delimit these previously well-defined mantle reservoirs; the "mantle zoo" may contain more reservoirs than previously envisaged.

However, here we demonstrate that a simple model with varying contributions from two populations of compositionally distinct mantle sulfides can readily account for the observed heterogeneities in Os isotope systematics of such basalts without additional mantle reservoirs. Osmium elemental and isotopic analyses of individual sulfide grains separated from spinel lherzolites from Kilbourne Hole, New Mexico, USA demonstrate that two discrete populations of mantle sulfide exist in terms of both Re-Os systematics and textural relationship with co-existing silicates. One population, with a rounded morphology, is preserved in silicate grains and typically possesses high [Os] and low [Re] with unradiogenic, typically sub-chondritic $^{187}Os/^{188}Os$ attributable to long term isolation in a low-Re environment. By contrast, irregular-shaped sulfides, preserved along silicate grain boundaries, possess low [Os], higher [Re] and a wider range of, but generally supra-chondritic $^{187}Os/^{188}Os$ ([Os] typically $\leq$ 1-2 ppm, $^{187}Os/^{188}Os \leq 0.3729$; this study). This population is thought to represent metasomatic sulfide.

Uncontaminated silicate phases contain negligible Os (<100 ppt) therefore the Os elemental and isotope composition of basalts is dominated by volumetrically insignificant sulfide ([Os] $\leq$ 37 ppm; this study). During the early stages of partial melting, supra-chondritic interstitial sulfides are mobilized and incorporated into the melt, adding their radiogenic $^{187}Os/^{188}Os$ signature. Only when sulfides armoured within silicates are exposed to

the melt through continued partial melting will enclosed sulfides add their high [Os] and unradiogenic $^{187}Os/^{188}Os$ to the aggregate melt. Platinum-group element data for whole rocks are also consistent with this scenario. The sequence of (i) addition of all of the metasomatic sulfide, followed by (ii) the incorporation of small amounts of armoured sulfide can thus account for the range of both [Os] and $^{187}Os/^{188}Os$ of EM-basalts worldwide without the need for contributions from additional silicate mantle reservoirs.

1. INTRODUCTION

Peridotite xenoliths are frequently entrained during the eruption of intra-plate magmas. Their utility in investigating mantle composition (e.g. Frey & Green, 1974; Ionov et al., 1993; Wilshire & Shervais, 1975; Stosch & Seck, 1980; Coisy & Nicolas, 1978; Stern et al., 1989) and basalt source reservoirs (e.g. Zindler & Hart, 1986; Hofmann, 1997) has been recognised for several decades. Their geographical dispersion is widespread and their accidental transport to the surface provides a means of sampling the mantle over a range of depths. Xenolith mineralogy, elemental composition, and isotope systematics all suggest that many peridotite xenolith suites have experienced varying degrees of partial melting (e.g. Jagoutz, et al., 1979; Galer & O'Nions, 1988) suggesting that suites of mantle xenoliths may be of particular utility in investigating the long term evolution and history of melt depletion in the mantle (e.g. Ross et al., 1954; Kuno & Aoki, 1970; Carlson & Irving, 1994; Pearson et al., 1995; Pearson, 1999; Griffin et al., 2003; Chu et al., 2009; Harvey et al., 2010).

Similarly, for several decades lithophile element-based isotope systems such as Sm-Nd, and Rb-Sr have been used to fingerprint the variable mantle sources (e.g. Galer & O'Nions, 1989) whose distinctive isotopic flavour is transferred to enriched-mantle (EM) basalts during partial melting. However, recent work involving the Re-Os isotope systematics of EM-basalts (e.g. Class et al., 2009) suggests that it may not be so simple to delimit these previously well defined mantle reservoirs; the "mantle zoo" (Stracke et al., 2005) may contain more reservoirs than previously envisaged. The commonly perceived understanding of how the Re-Os isotope system behaves during mantle melting is that the parent-daughter pair is unique due to the moderately incompatible and compatible nature of rhenium and osmium, respectively, on a bulk-rock scale (Pegram & Allègre, 1992); with rhenium, at least in part, residing within some silicate phases, e.g. garnet, based upon the observation that both Re and Yb concentrations are significantly higher in ocean island basalts (OIB) compared to

mid-ocean ridge basalts (MORB), i.e $D^{silicate/melt} \approx Yb$ (Hauri & Hart, 1997; Righter et al., 1998). However, in detail, the bulk-rock budget of Re, Os and the other platinum group elements (PGE), and critically the behaviour of these elements during partial melting, is decoupled from the mechanisms that control lithophile element-based isotope systems. Osmium within the Re-Os isotope system and PGE abundance are controlled, in the main, by volumetrically minor (<0.03 modal %) sulfide (Luguet et al., 2003; 2004).

At least two populations of sulfide are commonly found within peridotite samples from the upper mantle. Sulfide grains wholly enclosed within silicate grains, and effectively shielded from interaction or re-equilibration with metasomatic agents, possess supra-chondritic IPGE (Os, Ir, Ru) abundances, lower PPGE (Pt, Pd, Rh) and Re abundances and often retain sub-chondritic Os isotope ratios attributable to their long-term isolation from the silicate melt from which they immiscibly separated (e.g. Alard et al., 2002, 2005; Griffin et al., 2004; Bockrath et al., 2005; Mungall & Su, 2005; Harvey et al., 2006, 2010). Interstitial, or intergranular sulfides possess supra-chondritic abundances of Re and PPGEs, lower IPGE (Os, Ir, Ru) abundances and variable (sub- to supra-chondritic) Os isotope ratios, (e.g. Burton et al., 1999; Alard et al., 2002; Pearson et al., 2004; Bockrath et al., 2004; Mungall & Su, 2005; Harvey et al., 2006, 2010; Luguet et al., 2008). This population of sulfides has been demonstrated to be highly mobile during metasomatic events (e.g. Harvey et al., 2010), being easily mobilized and redistributed by transient melts and fluids. Hence, in the specific context of PGE distribution between these populations of sulfide and their Re-Os isotope characteristics the sub-oceanic and subcontinental lithospheric mantle (SCLM) are very similar (cf. Alard et al. 2005; Harvey et al., 2006; Liu et al. 2008; Luguet et al. 2008 for sub-oceanic lithospheric mantle and e.g. Burton et al., 1999; Alard et al. 2002; Harvey et al. 2010 for SCLM). It is also the early mobilization of interstitial sulfides during the onset of partial melting to which the apparent “isotopic gap” between mid-oceanic ridge basalts (e.g.,

Gannoun et al., 2004, 2007; Escrig et al., 2005), oceanic basalts (Reisberg et al., 1993; Roy-Barman & Allègre, 1995; Luguet et al., 2008) and abyssal peridotites (e.g., Alard et al., 2005; Harvey et al., 2006; Liu et al., 2008) has been attributed; a process that may also occur in SCLM settings and go at least some way to explaining the notoriously difficult interpretation of bulk rock rhenium-depletion (T_{RD}) ages (Rudnick & Walker, 2009).

This study presents bulk-rock PGE abundances and Re-Os elemental and isotope analyses of bulk-rock, silicate and spinel mineral separates, and 2 populations of sulfide in a suite of 28 peridotite xenoliths from Kilbourne Hole, New Mexico, USA. We demonstrate that the behaviour of the two compositionally and texturally distinct populations of peridotite-hosted sulfide controls the behaviour of Re and Os during partial melting. Moreover, using a simple two-stage model we demonstrate a means for the generation of the range of Re-Os elemental and isotopic compositions of worldwide EM-basalts without the need of additional mantle reservoirs to those proposed by Zindler & Hart (1986) and Hofmann (1997).

2. GEOLOGICAL SETTING, PETROLOGY AND PETROGRAPHY OF SAMPLES

Kilbourne Hole is one of several late Pleistocene volcanic maars situated in the Potrillo volcanic field on the axis of the Rio Grande Rift, an asymmetric system of grabens which extends for over 1000 km north – south through Colorado, New Mexico and Texas in the USA and onwards into Chihuahua, northern Mexico. The petrology and petrography of Kilbourne Hole mantle xenoliths have been the subject of extensive prior study, (e.g. Carter, 1965; Reid & Woods, 1978; Irving, 1979, 1980; Basaltic Volcanism Study Project, 1981; Bussod, 1981; Bussod & Irving, 1981). Mantle and crustal xenoliths are abundant in the lava flows in the Kilbourne Hole area. Dates for the eruption of the host basanite range from 80 Ka ± 10 Ka (Bussod & Williams, 1991; Thompson et al., 2005) to 141 Ka ± 75 Ka (Hoffer, 1976; Dromgoole & Pasteris, 1987) which suggests that any xenoliths exhumed at Kilbourne Hole have been separated from their source for only a relatively short period of geological time and are thus representative of the present-day mantle underlying the south-western USA.

The samples examined during the course of this study (n = 28) are Cr-diopside spinel lherzolites and spinel harzburgites with protogranular textures. A single sample (KH03-21) has a texture transitional between protogranular and porphyroclastic. Grain size is therefore generally greater than 1 mm and the samples are almost exclusively coarse grained. Porphyroclastic and granular xenoliths have also been reported at Kilbourne Hole. Although other petrographic textures have been observed (mosaic-porphyroclastic, tabular granular; Dromgoole & Pasteris, 1987; Kil & Wendlandt, 2004) textures other than protogranular are in fact rare at this locality and protogranular xenoliths are most representative of those recovered from Kilbourne Hole (Kil & Wendlandt, 2004).

Large (>1 kg) xenoliths were preferentially selected so that host basalt could be trimmed and the possible effects of host infiltration minimised while still retaining sufficient

material (>500 g) to represent a homogenous sample at the bulk-rock scale. The samples for this study were also selected so as to represent a wide range of clinopyroxene modal abundance, estimated visually in the field and subsequently calculated using a least squares regression method (Tarantola & Valette, 1982). Chrome-diopside modal abundance ranges from 3.3% to 17.2% (±1.6). No discrete metasomatic phases (e.g. phlogopite, amphibole, apatite) were detected during this study, or any prior study of this locality.

In addition to the silicate phases and spinel, which account for in excess of 99.97% of the volume of the samples, individual sulfide grains (n = 33) with bulk compositions broadly equivalent to pentlandite-rich and pentlandite-poor monosulfide solid solution (Luguet et al., 2003, 2004) were also analysed for major element abundances, Os abundances and Os isotopes.

3. ANALYTICAL METHODS

Samples were cut and washed to remove host basalt, surface alteration and contamination and rinsed in ultra-pure (>18 MΩ reverse osmosis scrubbed) water. Samples selected for bulk-rock analysis were dried and then powdered in an agate mortar. For the bulk-rock Re-Os measurements ~2 g of peridotite was dissolved in inverse aqua regia (3 mL 12M HCl / 9 mL 16M HNO_3) in sealed Carius tubes at 230°C for 7days (Shirey & Walker, 1995). A spike solution, enriched in ^{185}Re and ^{190}Os, was added immediately before the addition of the acids. Osmium was purified using CCl_4, leaving Re in the inverse aqua regia fraction (Cohen & Waters, 1996). The Os was subsequently recovered from the CCl_4 in HBr, microdistilled for 3 h at 90 °C (Birck et al., 1997) and dried down. Rhenium was extracted by drying down the inverse aqua regia and redissolving the residue in 2M Teflon-distilled HNO_3. The Re was recovered in iso-amylol (Birck et al., 1997), cleaned in a wash of 2M HNO_3 and finally extracted in ultrapure water. The reference material UB-N, a serpentinised peridotite, was digested numerous times (n = 6) to assess the efficacy of the Carius tube dissolution method for bulk-rock peridotite. Meisel et al. (2003) questioned "traditional" methods (i.e. low temperature acid attack; Carius tubes) for peridotite dissolution, citing resistant phases remaining undissolved which, in turn, led to poor reproducibility of Os concentrations and Os isotope ratios. Osmium concentrations of UB-N (3.4 to 4.2 ppb, n = 6) were indistinguishable from those obtained by high-pressure asher (e.g. Meisel et al., 2003), although the values obtained for the Os isotope ratio of UB-N were somewhat variable ($^{187}Os/^{188}Os$ = 0.1250 ± 2 to 0.1279 ± 1). However, repeat digestions of Kilbourne Hole bulk-rock samples (KH03-6, KH03-21 & KH03-25) by Carius tubes performed during this study demonstrate excellent reproducibility for both osmium concentrations and Os isotope ratios (e.g. KH03-06: [Os] = 1.54 ± 0.10 (2 sd); $^{187}Os/^{188}Os$ = 0.1269 ± 4 (2sd); n = 4). This suggests that the variability in the Os isotope measurements for UB-N obtained during this

study are more likely attributable to heterogeneity in the reference material, i.e. a nugget effect at the 2 g sample size, rather than artefacts attributable to incomplete digestion. Notwithstanding the possibility of either incomplete digestion or a nugget effect in the analysis of UB-N, neither of these factors appear to affect repeat analyses of Kilbourne Hole xenoliths. Reproducibility of Re concentrations in duplicate analyses is comparable to that achieved on corresponding Os measurements (KH03-21 [Re] = 0.08 ± 0.3 (2 s.d.) n = 4; KH03-10 [Re] = 0.23 ± 0.10 (2 s.d.) n = 2); KH03-6 [Re] = 0.07 ± 0.02 (2 s.d.) n = 4). Repeat digestions of reference material UB-N (n = 6) yielded Re concentrations of 0.184 ± 0.071 ppb, slightly below the preferred value of Meisel et al. (2003) which ranges from 0.201 to 0.241 ppb, although as stated above this likely reflects the heterogeneity of the reference material rather than inaccuracy of the measured concentration of a particular digestion. Reproducibility of Os isotope ratios in Kilbourne Hole bulk-rock peridotites is good. For example, repeat analyses of KH03-6 (n = 4) and KH03-21 (n = 3) differed by 0.14 % and 0.09 % respectively. Total procedural blanks for bulk-rock Os measurements during the course of this study were 3.85 ± 3.0 pg, $^{187}Os/^{188}Os = 0.170 \pm 0.031$, and for Re 1.85 ± 2.15 pg.

Aggregates of optically pure olivine, orthopyroxene, clinopyroxene and spinel were handpicked under a binocular microscope to ensure that both visible inclusions and surficial adherents were absent. The aggregates were repeatedly rinsed in analytical grade acetone and ultra-pure water before being powdered in an agate pestle and mortar. The powdered aggregates were then digested and Os and Re purified and recovered by low temperature acid attack, closely following the method described by Birck et al. (1997) and previously employed by Burton et al. (1999) and Harvey et al. (2010) on mineral phases from similar xenolithic material.

297 Rhenium–osmium chemistry for individual hand-picked sulfide grains was achieved
298 using a modified microdistillation technique that closely follows previously reported
299 procedures (Pearson et al., 1998). The total procedural blanks for Os in individual sulfides
300 were 0.10 ± 0.06 pg, $^{187}Os/^{188}Os$ = 0.36 ± 0.50, and for Re 3.14 ± 0.61 pg. Both Re and Os
301 samples were analysed on platinum filaments using negative thermal ionisation mass
302 spectrometry (N-TIMS) (Volkening et al., 1991; Creaser et al., 1991) using a
303 ThermoScientific Triton at The Open University, collecting individual masses by peak
304 jumping on a secondary electron multiplier. Long term accuracy of a Johnson Matthey
305 standard solution (14 pg to 8 ng; n = 85) is generally within 0.1% of the recommended values
306 for $^{187}Os/^{188}Os$. Typical signal intensities of ^{190}Os were in excess of 250,000 cps.
307 Bulk-rock PGE abundances of 6 peridotite xenoliths and the host basalt were
308 determined using the anion-exchange column procedures of Pearson & Woodland (2000) and
309 Dale et al. (2008). Bulk-rock powders were digested, together with a mixed PGE spike, in
310 inverse aqua regia (2.5 mL 12M HCl, 5 mL 16M HNO_3) in an Anton Paar high-pressure
311 asher. Following Os extraction by CCl_4, the inverse aqua regia was dried, refluxed in 12M
312 HCl and dried again. Chrome in its oxidised form (Cr^{6+}) can be present after aqua regia
313 digestion and behaves similarly to PGE on the anion exchange resin and hence can be eluted
314 with the PGE, causing polyatomic isobaric interferences on isotopes of Ru (Meisel et al.,
315 2008). Therefore, any Cr^{6+} present was reduced by the addition of H_2O_2, which was then
316 dried and the residue taken up in 10 mL of 0.5M HCl and loaded onto a column containing
317 AG1X-8 (100–200#) anion-exchange resin. The sample matrix was eluted with 10 mL of 1M
318 HF/1M HCl and 0.8M HNO_3 before Ir, Ru, Pt and Re were collected in 10 mL of 13.5M
319 HNO_3. Palladium was collected in 20 mL of 9M HCl after further elution of Zr using 1M
320 HF/1M HCl. Both the Ir–Pt–Ru–Re and the Pd cuts were dried down and taken up in 1 mL of
321 0.5M HCl for analysis using the ThermoScientific Element2 ICP-MS at Durham University.

Details of mass spectrometry procedures are given in Dale et al. (2008). The reproducibility of Ir, Pt and Pd abundances in the peridotite reference material GP13 is ~10% RSD, whereas Re has an uncertainty of 3% RSD. Reproducibility of IPGE, based upon multiple Os analyses of the peridotite samples is a maximum of ± 6% (2 σ).

4. RESULTS

4.1 Bulk rock Re and Os elemental and isotope measurements.

Bulk-rock Re concentrations ([Re]) range from 0.007 ppb to 0.693 ppb, with a mean concentration of 0.094 ppb (Table 1). The range of [Re] obtained during this study is much larger than that of Meisel et al. (2001) whose whole rock [Re] of samples from the same locality range from 0.053 ppb to 0.432 ppb. The mean [Re] from this study, like the mean Os concentration ([Os]), is significantly lower than the average mantle composition of 0.35 ppb (Becker et al., 2006) (Figure 1). Bulk-rock [Os] from this study (0.802 to 3.544 ppb, mean = 1.828; Table 1) are similar to previous studies of this locality (Morgan, 1986; Burton et al., 1999; Meisel et al., 2001) and studies of other peridotite suites from similar non-cratonic settings (e.g. Alard, 2002; Meisel et al., 2001; Liu et al., 2008; Ackerman et al., 2009; Harvey et al., 2010; Wittig et al., 2010) but are significantly lower than the mantle average (Becker et al., 2006).

The bulk-rock $^{187}Os/^{188}Os$ ratios of the samples range from 0.1159 to 0.1339 with a mean of 0.1256 (Table 1). All but 3 of the 28 xenoliths analysed have $^{187}Os/^{188}Os$ ratios <0.1296, the maximum present day estimate of the primitive upper mantle (PUM) of Meisel et al. (1996; 2001) and more than two thirds of the samples (n = 23) have sub-chondritic $^{187}Os/^{188}Os$ i.e. < 0.1270 (Walker & Morgan, 1989; Luck & Allègre, 1993). The values obtained in this study are similar to those from previous studies of this locality (Burton et al., 1999; Meisel et al., 2001) i.e. $^{187}Os/^{188}Os$ = 0.117 to 0.130, mean 0.1257, (n = 17). Whole rock $^{187}Re/^{188}Os$ ratios range from 0.009 to 1.35 with a mean of 0.222. However, only 3 samples, KH96-8, KH96-20 and KH96-24, have suprachondritic ratios (i.e. >0.4) and excluding these 3 samples gives a much narrower range of $^{187}Re/^{188}Os$ ratios (0.009 to 0.306,

369 mean = 0.156). This differs somewhat from previous work on xenoliths from the same
370 locality (Burton et al., 1999; Meisel et al., 2001) where the range of $^{187}Re/^{188}Os$ values was
371 0.228 to 0.781 and the mean much higher (0.395), i.e. near chondritic.

372 Figure 2a is a Re-Os isotope evolution diagram for the 28 bulk-rock peridotites from
373 this study. There is a broad positive co-variation between $^{187}Re/^{188}Os$ and $^{187}Os/^{188}Os$ and the
374 best fit line coincides with a calculated isochron age of 2.3 ± 0.7 Ga, but the relationship
375 cannot be described as convincingly isochronous despite, superficially at least, being in good
376 agreement with the ages derived from Sr isotope ratios of Roden et al. (1988) of 2.5 Ga ± 0.2
377 Ga for the SCLM beneath the south-western USA. On a bulk-rock scale Re has been
378 described as a moderately incompatible element during partial melting, contrasting with the
379 compatible bulk-rock behaviour of Os during melt depletion (Hart & Ravizza, 1996).
380 However, Re is mobile under a wide range of conditions (Meisel et al., 1996, 2001; Sun et
381 al., 2004), and the large degree of scatter on bulk-rock Re-Os isotope evolution diagrams can
382 be attributed, at least in part, to rhenium mobility. The best fit line in Figure 2a does not pass
383 through the estimated composition for PUM (Meisel et al., 2001) and the suite of samples
384 from this study appears displaced to a lower $^{187}Re/^{188}Os$ composition than those of Meisel et
385 al. (2001) supporting the notion that bulk rock Re may not behave in a systematic manner and
386 may be heterogeneous over spatially restricted areas.

387 A number of proxies for $^{187}Re/^{188}Os$ have therefore been sought amongst elements
388 that are not only moderately incompatible but also immobile and unaffected by secondary
389 processes not related to melt depletion. For example, Al, S and Yb (Reisberg et al., 2005;
390 Hauri & Hart, 1997; Burnham et al., 1998 respectively) are all believed to have similar bulk
391 partition coefficients to Re during partial melting but are generally considered to be immobile
392 at sub-magma generating temperatures. Figure 2b illustrates a much reduced degree of
393 scattering (R^2 = 0.89) between $^{187}Os/^{188}Os$ and Al_2O_3 and yields an "aluminachron" age

394 (Reisberg & Lorand, 1995) of 2.4 Ga, in good agreement with the best fit line through the Re-
395 Os isotope evolution diagram in Figure 2a and the Sr isotope age of Roden et al. (1988). We
396 expand on the subject of Re mobility below in the discussion of metasomatic sulfides and
397 their mobility.
398
399 **4.2 Bulk-rock PGE measurements**
400
401 Six peridotite xenoliths (KH03-10, KH03-15, KH03-16, KH03-18, KH03-21 &
402 KH03-24) that have experienced a wide range of melt depletion (1.1 to 4.4 wt.% bulk-rock
403 Al_2O_3) were selected for bulk-rock platinum-group element (PGE) measurements. In
404 addition, PGE abundances were also obtained for the host basalt. Bulk-rock PGE abundances
405 (Figure 3) are similar to those obtained elsewhere for non-cratonic lherzolites and
406 harzburgites (e.g. Lorand & Alard, 2001; Lorand et al., 2003; Wittig et al., 2010) but also
407 overlap with the lower end of PGE concentrations obtained from bulk-rock cratonic
408 peridotites (e.g. Pearson et al., 2004; Ivanov et al., 2008), orogenic massifs (e.g. van Acken et
409 al., 2010) and ophiolitic peridotite (Hanghøj et al., 2010). Osmium, iridium and ruthenium
410 (IPGE) abundances vary comparatively little within the samples analysed ([Os] = 1.39 to 3.36
411 ppb; [Ir] = 2.81 to 4.19 ppb; [Ru] = 4.77 to 7.47 ppb; Table 4) whereas Pt and Pd (PPGE),
412 along with Re, show much greater variability in elemental abundance ([Pt] = 3.35 to 6.58
413 ppb; [Pd] = 0.55 to 5.58 ppb; [Re] = 0.002 to 0.265 ppb; Table 4). While there is no strong
414 co-variation between indices of melt depletion (e.g. bulk-rock MgO or Al_2O_3) and PGE
415 abundance the more fertile peridotites do tend to contain higher abundances of PPGE than
416 less fertile samples, i.e. the fractionation of IPGE from PPGE appears, in general, to be most
417 pronounced in the most depleted peridotites, with Re being the most strongly fractionated
418 from the IPGEs.

4.3 Re-Os abundance and isotope ratios of silicate minerals and spinel

Optically pure mineral separates of olivine, orthopyroxene and clinopyroxene, spinel and individual sulfide grains were handpicked from 4 xenoliths, KH03-15, KH03-16, KH03-21 and KH03-24. These samples were selected on the basis of their wide range of modal abundance of clinopyroxene (2.5 to 17.5 modal %). Osmium concentrations of the silicate phases are presented in Table 2. The high [Os] of clinopyroxene from KH03-16 is probably derived from contamination from one or more microscopic sulfide grains enclosed within the clinopyroxene (surficial contamination, if unobservable during the picking, would probably have been removed during the cleaning process). Osmium concentrations in spinel are up to an order of magnitude more Os than many of the co-existing silicate phases. It is difficult to assess the origin of the high [Os] of spinel as its opaque nature makes it impossible to guarantee that handpicked grains are free from sulfide inclusions. With the exception of presumably contaminated clinopyroxene from KH03-16, [Os] increases in the following manner: olivine < orthopyroxene < clinopyroxene < spinel.

Rhenium concentrations of the same silicates are also presented in Table 2. Spinel tends to have higher [Re] than the silicate phases (47.1 ppt to 818 ppt) (Table 2). While spinel invariably contains the greatest [Re], the distribution of Re amongst the silicate phases is not as clear as the relationship shown for [Os] above. Olivine has the lowest [Re] in all 4 of the samples and the two pyroxenes have a lower [Re] than spinel (other than clinopyroxene from KH03-16, which may be contaminated by sulfide). Although the experimental results of Mallmann & O'Neill (2007) and Righter et al. (2004) suggest that Re does partition into clinopyroxene to a certain extent, the relative partitioning of Re between the pyroxenes in this study is not systematic. The Os isotope ratios and $^{187}Re/^{188}Os$ ratios for silicate mineral

444 separates are presented in Table 2. In all cases Os isotope ratios of mineral separates are
445 higher than the corresponding bulk-rock values. Because of the large uncertainties on the
446 mineral Re-Os isochrons no meaningful age information is preserved in the silicate phases
447 alone.

448 The presence of contamination from included sulfide grains in clinopyroxene from
449 KH03-16 raises the question of whether all of the [Re] and [Os] for mineral separates from
450 this study can be accounted for by varying degrees of sulfide contamination. Burton et al.
451 (1999) demonstrated the effect of included sulfides upon the Os elemental and isotope ratio
452 of a mineral separate. In their study, minerals with sulfide contamination have elevated [Os]
453 (an order of magnitude greater than their clean mineral separates) and Os isotope ratios were
454 indistinguishable from the bulk-rock value. Osmium concentrations of clean mineral
455 separates from this study are similar to those obtained by Burton et al. (1999). The
456 probability of the same degree of sulfide contamination in mineral separates from
457 independent studies is very small. Similarly, the sequential increase in concentration from
458 olivine, through orthopyroxene and clinopyroxene to spinel from all 4 samples from this
459 study (with the exception of KH03-16 clinopyroxene) is difficult to account for with the [Os]
460 being solely attributed to contamination from sulfide inclusions.

461

462 **4.4. Major element abundances, Re-Os concentration and isotope systematics of**
463 **individual sulfide grains.**

464

465 *4.4.1 Major element abundances of individual sulfide grains*

466

467 Based upon the relative proportions of Ni, Fe and Cu, three populations of sulfide
468 have been identified in the Kilbourne Hole xenoliths from this study (Figure 4). Two of the

populations have low Cu abundance (0.08 to 4.68 wt %) and are defined by either a high or low Fe:Ni ratio. Major element abundances of 57 sulfides derived by electron microprobe are given in Table 3. These two populations are broadly equivalent to pentlandite-rich and pentlandite-poor monosulfide solid solution (MSS) sulfides (Luguet et al., 2003, 2004). Within the MSS sulfides analysed there is a broad inverse co-variation between Ni and Fe abundances. The third population of sulfide is characterised by a significantly higher Cu abundance, analogous to chalcopyrite rich sulfides from previous studies (Dromgoole & Pasteris, 1987; Luguet et al., 2003, 2004).

High-Cu sulfides from this study have very high Fe:Ni ratios and plot significantly below the array of the monosulfide solid solution samples. The relative proportion of Ni, Fe, and Cu in sulfides has implications for the capacity of a sulfide to host Os. Monosulfide solid solution with higher Ni content has a greater proportion of octahedral sites in which Os is commonly hosted (Mackovicky et al., 1986; Cabri, 1999; Ballhaus et al., 1999). A single sulfide with a composition similar to that of the basalt hosted sulfide of Burton et al. (1999) is also illustrated in Figure 4. However, in this instance the sulfide is located within a peridotite xenolith (KH03-23) rather than the host basalt suggesting that some degree of infiltration of and interaction with the host lava itself has occurred (Hammond et al., 2010).

4.4.2. Re-Os concentration and isotope systematics of individual sulfide grains

Individual sulfide grains have by far the highest Os content of any of the constituent phases of mantle xenoliths. All of the xenoliths from which mineral separates were picked contain sulfides with [Os] several orders of magnitude greater than any of the co-existing silicates or spinel. A total of 33 individual sulfide grains were analysed: KH03-15 (n = 7), KH03-16 (n = 7), KH03-21 (n = 10) and KH03-24 (n = 9). Their [Os] vary from 0.001 ppm

494 to 36.85 ppm (Table 5). Rhenium concentrations of the sulfide grains are also high and, in
495 general, orders of magnitude greater than the silicate phases and spinel. Rhenium
496 concentrations for 19 sulfide grains were obtained during this study (KH03-15, n = 4; KH03-
497 16, n = 5; KH03-21, n = 4; KH03-24, n = 6) which range from 0.002 ppm to 138.9 ppm
498 (Figure 6). Curiously, sulfide grains from relatively fertile samples (KH03-21 and KH03-24)
499 have a narrow range of [Os] but a wide range of [Re] and sulfide grains from depleted,
500 metasomatised samples (KH03-15 and KH03-16) show the opposite i.e. a wide range of [Os]
501 but a restricted range of [Re].

502 The morphology of each individual grain was assessed in an attempt to determine the
503 textural location of the sulfide prior to disaggregation of the xenolith and hand-picking of the
504 grain. The separated grains were categorised as either euhedral / rounded / subrounded, or
505 anhedral / subhedral / irregular. The former were inferred to have originated as grains
506 armoured within individual silicate grains while the latter were ascribed to an interstitial
507 origin (Alard et al., 2002). Euhedral / rounded / subrounded grains tend to have high Os
508 concentration and low Re concentrations while the converse is generally true in the anhedral /
509 subhedral / irregular grains.

510 The 33 individual sulfide grains have Os isotope ratios ranging from 0.1185 to
511 0.3729. Sulfides from individual xenoliths also have a wide range of $^{187}Os/^{188}Os$ ratios (Table
512 5). Within the entire sulfide population there is a broad inverse trend between Os isotope ratio
513 and [Os], i.e. grains with the highest [Os] are frequently the least radiogenic and *vice versa*
514 (Figure 5). Although the trend as a whole is less clear in the bulk-rock measurements, Figure
515 5b illustrates that the samples with the highest bulk-rock [Os] also tend towards the lower Os
516 isotope ratios. Enclosed sulfide grains, which are often rounded, subrounded or euhedral in
517 shape, have uniformly low $^{187}Os/^{188}Os$ values that are slightly below or indistinguishable
518 from the bulk-rock Os isotope ratio (Figure 5b) and commonly have the highest [Os] and low

[Re]. Interstitial sulfide grains are often anhedral, irregular or subangular shaped and, like the silicate and spinel mineral separates, are characterised by Os isotope ratios that exceed those of the corresponding bulk- rock value. They have much lower [Os] and higher [Re] than the other sulfide population. That the silicate minerals and interstitial sulfides in many cases yield similar Os isotope compositions for a range of Re/Os ratios suggests a degree of recently attained isotopic equilibrium (cf. Burton et al., 1999).

5. DISCUSSION

5.1. Bulk rock Re-Os isotope systematics during partial melting.

The commonly held perception of the behaviour of Re and Os on a bulk-rock scale is that Os behaves as a compatible element during partial melting of the mantle. This contrasts with Re which behaves as a moderately incompatible element (e.g. $D_{Re}^{opx/melt}$ = 0.013, $D_{Re}^{cpx/melt}$ = 0.18–0.21; Righter et al., 2004). A first order prediction therefore would be that this will result in a residue that, after melt extraction, retains a moderately high Os content yet is significantly depleted in Re; almost complete exhaustion of Re can be expected with continued melt depletion. In the absence of subsequent metasomatism, evidence for prior melt depletion should therefore be preserved within, for example, peridotite xenoliths and will be characterized by unradiogenic, i.e. sub-chondritic Os isotope ratios ($^{187}Os/^{188}Os$ <0.1270; Luck & Allègre 1983; Walker & Morgan, 1989). However, metasomatism occurring after melt depletion has the effect of obscuring the primary Os isotope signature of ancient melt depletion. This may take the form of addition of ^{187}Os from material recycled back into the asthenosphere or by adding metasomatic Re which, over time, will generate radiogenic ^{187}Os, thus shifting bulk-rock $^{187}Os/^{188}Os$ to higher values.

Conversely, enriched-mantle (EM) basalts produced by the partial melting of peridotite generally contain significantly less Os than peridotite (often < 10 ppt, average [Os] = 428 ppt; Reisberg et al., 1993; Roy-Barman & Allègre, 1995; Martin et al., 1994; Bennett et al., 1996; Hauri & Kurz, 1996; Hauri et al., 1996; Lassiter & Hauri, 1998; Widom et al., 1999; Brandon et al., 1999, 2007; Lassiter et al., 2000, 2003; Skovgaard et al., 2001; Eisele et al., 2002; Workmann et al., 2004; Gaffney et al., 2005; Jamais et al., 2008; Debaille et al., 2009; Day et al., 2009; Class et al., 2009), but occasionally extend to values comparable with those of peridotite samples (e.g. >4.4 ppb; Ireland et al., 2009). Although isolated EM-basalts

585 have relatively unradiogenic $^{187}Os/^{188}Os$ (e.g. as low as 0.1212; Debaille et al., 2009) in
586 general EM-basalts have radiogenic Os isotope ratios, extending to $^{187}Os/^{188}Os$ = 0.2621
587 (Ireland et al., 2009). All of these observations are consistent with, on a bulk-rock scale, Os
588 behaving as a compatible element during partial melting and the moderately incompatible
589 nature of Re. When plotted against a reliable index of melt depletion, e.g. bulk-rock Al_2O_3
590 wt%, peridotite Os isotope ratios seem to co-vary with the effects of the extraction of
591 increasing amounts of basaltic melt (e.g. Reisberg & Lorand, 1995). Lower Os isotope ratios
592 coupled with low Al_2O_3 wt% would seem consistent with the early and efficient removal of
593 Re during melt depletion and a lack then of radiogenic ingrowth of ^{187}Os – a process masked
594 in Figure 2a by the subsequent addition of metasomatic Re but seemingly stripped away by
595 using a suitable proxy for melt depletion in Figure 2b.
596 However in detail, Os elemental abundances of, in particular, non-cratonic xenoliths
597 such as those from this study, and other non-cratonic xenolith localities worldwide, are
598 simply not consistent with the notion that on a bulk-rock scale Os behaves as a compatible
599 element during partial melting. What is inconsistent with this hypothesis is that only 1 sample
600 from this study and 3 samples in total, from 42 samples in 4 separate studies of this locality
601 (Morgan, 1986; Burton et al., 1999; Meisel et al., 2001; this study) have [Os] that are higher
602 than a nominally fertile mantle – a characteristic that should be the norm rather than the
603 exception if Os behaves compatibly on a bulk-rock scale during partial melting. In effect,
604 there is a significant deficiency of [Os] in bulk-rock peridotite if Os behaves in a compatible
605 manner during melt depletion and if this is the main control on the behaviour of this element.
606
607
608
609

610 **5.2 Osmium mass balance in peridotites**

611

612 Several earlier studies (Hart & Ravizza, 1996; Burton et al., 1999; Harvey et al.,
613 2010) have demonstrated that the contribution to the [Os] of bulk-rock peridotites derived
614 from the major rock-forming minerals (olivine, orthopyroxene, clinopyroxene, spinel) is
615 negligible. In optically pure hand-picked aggregates of these minerals from this study no
616 more than 5% of bulk-rock Os can be accounted for from these phases. This is consistent
617 with previous experimental studies (e.g. Fleet et al., 1991, 1996, Brenan et al., 2003, 2005)
618 which determined the relative affinities of Os and the other PGE between sulfide and silicate
619 assemblages. The experimentally derived partition coefficients for Os between sulfide and
620 silicate liquids ($D_{Os}^{sulfide/silicate}$) of 10^4 to 10^6 are supported by the [Os] measured in optically
621 pure silicate phases and hand-picked individual sulfide grains of this study (Table 5). Thus,
622 volumetrically insignificant sulfides account for >95% of the Os mass balance of peridotite
623 xenoliths. It is the behaviour of sulfide during melt depletion that will determine the Os
624 abundance and isotope systematics of a basalt formed by the partial melting of a
625 predominantly silicate pre-cursor source rock. However, compositional heterogeneity exists
626 within mantle sulfide populations; Alard et al. (2002) and Pearson et al. (2002) identified two
627 distinct sulfide populations based upon their morphology, [Os], $^{187}Os/^{188}Os$, [Re] and textural
628 constraints. Sulfides that appear to be entirely enclosed within silicate grains, and thus
629 protected from any subsequent interaction with melts or fluids tend to be rounded to sub-
630 rounded, have high Os concentration ([Os] = 10s ppm), unradiogenic (sub-chondritic)
631 $^{187}Os/^{188}Os$) and low [Re], thus reflecting a long term evolution in a low-Re environment and
632 probably representing the separation of an immiscible sulfide liquid during a previous melt
633 depletion event (e.g. Holzheid, 2010). This is consistent with the findings of Bockrath et al.
634 (2004) and Mungall & Su (2005) where Os-Ir-Ru rich sulfides remained in a peridotite

635 residue because of their tendency to adhere to silicate grains. This also supports the notion
636 that enclosed sulfides are the result of an immiscible sulfide liquid that separated from a co-
637 existing silicate liquid during fractional crystallisation of an early melt; the sulfides being
638 preserved within early forming silicate phases. In contrast, a second population of sulfides
639 occupies interstitial and intergranular locations within the peridotite. Their composition is
640 somewhat different to the first population; [Os] is frequently at the sub-ppm level, [Re] is
641 higher and more variable than enclosed sulfides and consequently $^{187}Os/^{188}Os$ of these
642 sulfides is more radiogenic, i.e. variable and supra-chondritic, even within a population
643 recovered from a single xenolith (Table 5). The textural relationship of these sulfides with
644 silicate phases suggests that this population of sulfides are secondary and most likely derived
645 from a metasomatic event subsequent to melt depletion. While sulfides entirely enclosed
646 within silicate grains tend to evolve under closed system conditions, interstitial sulfides, by
647 virtue of their textural location in the peridotite, experience open system behaviour and are
648 prone to melting, dissolution or physical displacement by any transient melt or fluid. As such,
649 their composition can be modified by mixing of interstitial sulfides of different ages and / or
650 Re/Os ratios, possibly accounting for the wide range of Re/Os ratios in interstitial sulfides.
651 This is notwithstanding the possible additions to the Re and Os budget of interstitial sulfides
652 from Re and / or radiogenic Os fluxed from basaltic material mixed back into the convecting
653 mantle, although the relative quantity of these elements in interstitial sulfides from this source
654 is difficult to quantify. The logical extension of these observations is that bulk-rock Re-Os
655 systematics of peridotite xenoliths will therefore be governed by the relative proportions of
656 these two sulfide populations; the exact nature of an individual xenolith being determined by
657 the abundance of each sulfide population. Figure 6 demonstrates the contribution of these two
658 populations of sulfide in four samples from this study. Mass balance calculations show that in
659 most cases the difference in [Os] between sulfide populations is sufficiently high that,

660 assuming similar abundances of each population, the contribution from low concentration,
661 interstitial (i.e. metasomatic) sulfide is small and does not markedly affect the whole rock Os
662 isotope ratio. Figure 6 also confirms that the proportion of whole rock Os that can be
663 accounted for by the contributions of olivine, orthopyroxene, clinopyroxene and spinel in 4
664 samples from this study is <5 % of the whole rock Os budget and in the case of KH03-21 as
665 little as 2.4 %.

666 While a simple mass balance calculation reveals that KH03-24 does not require a
667 contribution from interstitial sulfides to account for its measured bulk-rock Os abundance and
668 isotope ratio, radiogenic interstitial sulfides with low [Os], high [Re], were sampled from this
669 xenolith (Table 5). Consequently, this suggests that the significantly greater [Os] of enclosed
670 sulfides vastly outweighs the contribution to the Os budget of the interstitial grains. The
671 majority of the sulfide grains analysed from KH03-16 are interstitial (see Table 5). However,
672 to balance the bulk-rock Os isotope ratio of KH03-16 an unradiogenic component is required.
673 Bulk-rock S analyses, which limit the amount of sulfide available for mass balance
674 calculations, suggests that as little as 0.02 wt % of typical enclosed sulfide would balance the
675 whole rock Os isotope ratio and Os concentration of xenolith KH03-16. However the most
676 unradiogenic enclosed sulfides, which must be present, were not recovered from this
677 xenolith. Therefore, the contribution to the bulk rock Os budget from each population of
678 sulfide can only be estimated for KH03-16. In order to balance the whole rock Os isotope
679 ratio the interstitial sulfides cannot contribute more than 17.5 % of the whole rock budget, but
680 with the knowledge of the [Os] of enclosed sulfides from other Kilbourne Hole xenoliths the
681 contribution from interstitial sulfides is probably significantly less. The Os isotope ratio of
682 KH03-15 is too radiogenic be accounted for by the sum of the contributions from the silicates
683 and spinel plus an overwhelming contribution from enclosed sulfides alone. A relative
684 contribution of 3.5% from interstitial sulfide is sufficient to balance the bulk-rock Os isotope

685 ratio and bulk-rock [Os]. A similar calculation to that of KH03-15 is required for KH03-21,
686 except a greater contribution (<17.5 %) must come from interstitial sulfides to balance the
687 whole rock Os systematics. When metasomatic, interstitial sulfide is present in these
688 quantities bulk-rock $^{187}Os/^{188}Os$ will deviate significantly from the Os isotope signature of a
689 xenolith whose [Os] is dominated by enclosed sulfides.

690 With the exception of KH03-21, the effects of metasomatic, interstitial sulfide on the
691 Os isotope ratio of the whole rock are of little consequence. Only in samples where the
692 abundance of radiogenic, low [Os], interstitial sulfide is so great as to skew the whole rock
693 Os isotope ratio are whole rock $^{187}Os/^{188}Os$ ratios unrepresentative of their enclosed sulfides.
694 Nevertheless, in peridotites xenoliths elsewhere, when the abundance of interstitial
695 metasomatic sulfides is higher, an early melt depletion signature may easily be obscured and
696 bulk-rock Re-Os systematics will only describe a mixture of metasomatic sulfide and earlier
697 melt depletion-related sulfides, thus yielding nothing more than a meaningless "average" Os
698 isotope ratio. For example, bulk-rock T_{RD} can vastly underestimate the timing of melt
699 depletion by up to 0.5 Ga (e.g. Harvey et al., 2006). Figure 7 illustrates the relationship
700 between bulk-rock Re-Os systematics of KH03-15, KH03-16, KH03-21 and KH03-24 and
701 their constituent components. In all cases the bulk-rock $^{187}Os/^{188}Os$ appears to be strongly
702 controlled by enclosed sulfides, mainly as a result of their high [Os] (Table 5). In general, the
703 xenoliths appear to have at least one silicate phase that resembles the $^{187}Os/^{188}Os$ of the bulk-
704 rock. However the [Os] of these phases (Table 3 and Figure 7) is insufficient to exert a
705 significant control on bulk rock [Os] and therefore bulk-rock $^{187}Os/^{188}Os$. Consequently, in
706 peridotite xenoliths in general, bulk-rock T_{RD} ages are often unlikely to reflect an early melt
707 depletion event, especially when a large proportion of the peridotite sulfide budget comes
708 from the interstitial, secondary or metasomatic population. A more accurate appraisal of early
709 melt depletion is more likely derived from the analysis of individual enclosed sulfide grains

710 that have been protected from subsequent metasomatism. For example, the bulk-rock T_{RD} age
711 of KH03-15 (Table 1) underestimates the age of the oldest sulfide analysed from the same
712 bulk-rock sample by >400 Ma. Similarly, the bulk-rock T_{RD} age of KH03-24 is 150 Ma
713 younger than the oldest enclosed sulfide recovered from that xenolith.

714 The low sulphur concentrations of the Kilbourne Hole xenoliths of this study suggests
715 that a large proportion of their original sulphur has been lost prior to transport to the surface
716 in the host basalt. Sulphur concentrations for KH03-15, KH03-16, KH03-21 and KH03-24
717 are all below 50 ppm (KH03-16 [S] <10 ppm), significantly below that expected for fertile
718 mantle ([S] = 200 ± 40 ppm, O'Neil, 1991). Consequently, as sulfide is likely the dominant
719 phase for [S] in peridotite this implies that a significant proportion of sulfide has also been
720 lost, which may, at least in part, account for the low [Os] when compared to the primitive
721 mantle. However, low [S] is not ubiquitous in sub-continental lithospheric mantle xenoliths
722 and therefore this mechanism is unlikely to be universal (e.g. Reisberg et al., 2005).
723 Moreover, the interstitial nature of one of the populations of sulfide suggests that it is more
724 likely to be mobile and prone to alteration under a wide range of circumstances, e.g.
725 supergene weathering (e.g. Lorand et al., 2003), melt depletion and / or metasomatism (e.g.
726 Handler et al., 1999) than those sulfides enclosed within a host silicate grain with no
727 exposure to grain boundary processes.

728

729 **5.3 Control of HSE abundances by multiple sulfide populations during partial melting**

730

731 *5.3.1 Osmium concentrations and $^{187}Os/^{188}Os$ in EM-basalts*

732

733 The generation of basaltic magma requires partial melting of a peridotite precursor
734 material, the exact melt composition being dependent upon the pressure, temperature, fO_2 and

735 the composition of the source reservoir. It is, for instance, the variability in the composition
736 of EM-basalts that has often been attributed to the variability in the source material; their
737 heterogeneity being ascribed to various discrete, yet compositionally distinct mantle
738 reservoirs variously refertilised or enriched with recycled basaltic and / or sedimentary
739 material as a result of ongoing subduction and mixing (Zindler & Hart, 1986; Hofmann
740 1997). The contrasting physical properties of these re-introduced components has been
741 suggested to be responsible for their resistance to complete re-mixing back into the
742 asthenospheric mantle to produce a single homogeneous reservoir from which subsequent
743 basalt can be extracted (e.g. Allègre & Turcotte, 1986; Hart, 1988; Manga, 1996). It has long
744 been accepted that the re-melting of these recycled components generates the distinctive
745 isotopic flavour of the various EM-basalts; their Sr-Nd-Pb isotope composition being
746 geographically restricted and reflecting the mixture of melt derived from asthenospheric
747 mantle and its enriched sub-reservoirs. While this explanation of EM-basalt heterogeneity is
748 robust for isotope systems that are reliant upon lithophile elements (Rb-Sr, Sm-Nd, Pb-Pb,
749 etc) it has recently been suggested that in order to account for the wide range of Re-Os
750 isotope heterogeneity in EM-basalts, and Grande Comore EM-basalts in particular (e.g. Class
751 et al., 2009), additional enriched mantle reservoirs are required.

752 Despite the apparent incompatibility of Os in silicate minerals, demonstrated both
753 experimentally (Fleet et al., 1991, 1996; Brenan et al., 2003, 2005) and measured in natural
754 samples (Hart & Ravizza, 1996; Burton et al., 1999; Harvey et al., 2010; this study) there is
755 insufficient Os within the silicate phases to produce a significant volume of EM-basalt with
756 the observed range of [Os], even at very low degrees of partial melting – the meagre Os
757 budget in the silicate minerals is quickly exhausted and massively diluted during the melting
758 of the silicate phases. This is in contrast to the lithophile element-based isotope systems
759 whose parent and daughter elements (e.g. Rb, Sr, Sm, Nd, U, Pb) are present in much greater

760 abundances within the silicate minerals that produce the basaltic melt. The Os budget of EM-
761 basalts is much more likely derived from mantle sulfide which hosts the vast majority of
762 mantle Os. Mobilisation of this sulfide and its incorporation into a basaltic partial melt is
763 therefore a far more plausible mechanism for producing a wide range of Os isotope ratios in
764 EM-basalts and, moreover, the wide range of [Os] observed worldwide. A simple two stage
765 model demonstrates that the entire range of EM-basalt Os isotope and elemental abundances
766 can be produced by the sequential incorporation of (i) interstitial sulfide with sub ppm [Os]
767 and radiogenic $^{187}Os/^{188}Os$ followed by (ii) the gradual addition of sulfide grains formerly
768 enclosed within silicate grains which, as melt depletion intensifies, become exposed to the
769 melting process as their host grains themselves start to melt. These formerly enclosed
770 sulfides, randomly oriented within their host grains, then contribute their high [Os] and
771 comparatively unradiogenic $^{187}Os/^{188}Os$ to the basaltic melt. Figure 8 illustrates this process
772 and demonstrates schematically that with a representative range of mantle sulfides the entire
773 range of both [Os] and Os isotope ratios can be produced from simple batch melting. As
774 discussed above, melting of the silicate minerals can only produce a very limited range of
775 [Os] and will not account for any great variability in $^{187}Os/^{188}Os$ given a broadly chondritic
776 starting material. The range of melt compositions from the silicate components alone is
777 shown in Figure 10 (white box). This is derived from 1-10 % batch melting of sulfide-free
778 silicates whose compositions were determined in this study, Burton et al. (1999) and Harvey
779 et al. (2010). A very limited range of small volume melts can be produced even when
780 $D_{Os}^{silicate/melt}$ is varied by up to an order of magnitude. Interstitial sulfide, with its particularly
781 low melting temperature compared to that of silicate minerals (Hsieh et al., 1987; Eggler and
782 Lorand, 1993), will become mobilized and incorporated into the melt very early in the partial
783 melting process. As soon as melt forms an interconnected network around grain boundaries
784 then the contribution of interstitial sulfide to the Os budget of the basalt can be added

785 (process 1 on Figure 8). However, this may only occur at higher temperatures than those at
786 which sulfide would physically melt (e.g. Bockrath et al., 2004; Ballhaus et al. 2006) as
787 sufficient silicate melting will need to occur before sulfide can be mobilised (the mobility of
788 interstitial sulfide in silicate melts during partial melting is summarized in Rudnick &
789 Walker, 2009). With continuing melt depletion enclosed sulfide grains, randomly oriented
790 with regard to their proximity to silicate grain boundaries, will progressively be exposed and
791 thus incorporated into the melt, rapidly increasing the basalt [Os] and lowering the overall
792 $^{187}Os/^{188}Os$ (process 2, Figure 10). For example, using the range of [Os] and $^{187}Os/^{188}Os$ for
793 Kilbourne Hole interstitial sulfides alone it is possible to produce basalts with a range of Os
794 isotope ratios between approximately that of primitive upper mantle (PUM $^{187}Os/^{188}Os$ =
795 0.130; Meisel et al., 2001) and 0.170, and with [Os] of <100 ppt to c. 270 ppt. This is readily
796 achieved by mixing the results of up to 10% batch melting of a typical PUM silicate
797 assemblage and adding less than 0.01 modal % of Kilbourne Hole interstitial sulfide, i.e. an
798 amount of sulfide well within the range of modal abundances measured by e.g. Luguet et al.
799 (2003). Using the range of cratonic sulfides from Griffin et al., (2004), the full range of Os
800 elemental and isotope systematics of Comores EM-basalts, the extreme $^{187}Os/^{188}Os$ end-
801 member of EM-basalt, can be generated with an order of magnitude less sulfide. The range of
802 higher [Os] and less radiogenic EM-basalts is then easily accommodated by the gradual
803 addition of formerly enclosed sulfides with high [Os] and generally sub-chondritic
804 $^{187}Os/^{188}Os$. Although only two examples are calculated here these two solutions are not
805 numerically unique and various combinations of geologically reasonable sulfide populations
806 with both normal [Os] and $^{187}Os/^{188}Os$ allow the Os systematics of the full range of EM-
807 basalts, and most ocean island basalts (OIB) in general to be generated.
808
809 *5.3.2 The influence of sulfide on EM-basalt PGE systematics*

The early mobilisation of interstitial sulfides followed by the later incorporation of formerly enclosed sulfides is also supported by the observed behaviour of other platinum group elements (PGE). Previous studies of the two discrete populations of mantle sulfides have shown that Os-rich enclosed sulfides are also rich in Ir and Ru (IPGEs) but, compared to interstitial sulfides, are depleted in Pt, Pd (PPGEs) and, as previously discussed, Re (Lorand & Alard, 2001; Aulbach et al., 2004; Bockrath et al., 2004; Mungall & Su, 2005). The early incorporation of PPGEs into MORB has also been demonstrated to be responsible for the apparent PGE and Os-isotopic gap between MORB, ocean island basalts (OIB) and their mantle sources (Alard et al., 2005; Luguet et al., 2008). Consequently, the behaviour of any two IPGE in bulk-rock peridotite during partial melting should be strongly correlated, as should that of any two PPGE as the two populations of sulfide, each with a distinctive composition, contribute to the basaltic melt in a predictable, but different way. Conversely, it would be expected that no significant correlation would be observed between an IPGE and a PPGE in peridotites over an interval of melt depletion. Figure 9a demonstrates an excellent correlation in bulk-rock peridotite abundances of pairs of IPGE, i.e. Ir_N vs. Os_N & (where X_N is [X] normalised to the composition of CI chondrite, after Horan et al., 2003) over the range of melt depletion experienced by the peridotites of this study. Similarly PPGE, e.g. Pd_N vs. Pt_N, demonstrate a similar behaviour ($R^2 > 0.9$, with the exclusion of KH03-16), albeit because of the mobilization of a different sulfide population. However, very little co-variation between individual IPGE vs. individual PPGE exists (Pt_N vs. Os_N). This strongly suggests that the behaviour of IPGE and PPGE during melt depletion is controlled by different phases, i.e. the two compositionally distinct populations of interstitial (high PPGE/IPGE) and enclosed (low PPGE/IPGE) sulfide. This observation is not unique to this particular locality and although the co-variation is not as statistically robust when worldwide peridotites are

835 considered (Figure 9b) the positive co-variation between individual IPGE is still evident in
836 other non-cratonic peridotite xenoliths (Lorand & Alard, 2001; Lorand et al., 2003; Wittig et
837 al, 2010), cratonic peridotite xenoliths (Pearson et al., 2004; Ivanov et al., 2008), orogenic
838 peridotites (e.g. van Acken et al., 2010), abyssal peridotites (e.g. Luguet et al., 2001, 2003,
839 2004) and ophiolitic peridotite (Hanghøj et al., 2010). The notion that IPGE and PPGE
840 mobility, and hence their contribution to basaltic magmas during partial melting of peridotite,
841 is controlled by two separate phases is also supported by the PGE distribution amongst
842 mantle sulfides themselves. Strong correlations between Ir_N vs. Os_N ($R^2 > 0.99$) in sulfides
843 from non-cratonic peridotite (Lorand & Alard, 2001), cratonic peridotite (Aulbach et al.,
844 2004) and abyssal peridotites (Luguet et al., 2001, 2003, 2004) are evident (Figure 9c) and
845 demonstrate that sulfide is the primary control on the behaviour of PGE and Re during melt
846 extraction. Although the co-variation is not as strong between sulfide PPGE, the general trend
847 is still compelling. The net result of the preferential incorporation initially of interstitial
848 sulfide followed by the gradual addition of enclosed sulfide with increasing degrees of partial
849 melting is then clear. The strong correlations between paired IPGE and paired PPGE in
850 peridotitic sulfide (Figure 9c) and lack of correlation between individual IPGE and PPGE
851 illustrates that the two populations of sulfide are the main control on PGE abundance in
852 peridotites not just from this study (Figure 9a) but non-cratonic, cratonic, abyssal and
853 ophiolitic peridotites worldwide (Figure 9b). Moreover, the consistent and predictable
854 behaviour of mantle sulfide during partial melting is evident when the PGE composition of
855 worldwide basalts are examined; the same consistent behaviour of IPGE and PPGE is also
856 evident in basalts irrespective of tectonic setting (Figure 9d) – the PGE abundances and Os
857 isotope composition of basaltic magma can be explained simply by the contribution of first
858 one population of sulfide, with a high PPGE/IPGE, followed by gradual addition of formerly
859 enclosed sulfide with low PPGE/IPGE controls.

860 Using continental peridotites to derive the composition of oceanic basalts may not
861 always be appropriate as SCLM has invariably been isolated from the convecting mantle for
862 longer and hence likely experienced more metasomatic input than its sub-oceanic counterpart.
863 However, in the case of the peridotites used for this study the choice of material appears
864 justified. In selecting petrographically and texturally simple peridotites that last equilibrated
865 at or near the local asthenosphere / lithosphere boundary the protogranular lherzolites and
866 harzburgites share a number of features with similar oceanic peridotites. Mean Os isotope
867 ratios for abyssal peridotites ($^{187}Os/^{188}Os$ = 0.1236; Snow & Reisberg, 1995; Brandon et al.,
868 2000; Harvey et al., 2006; Liu et al., 2008) are similar to the Kilbourne Hole peridotites used
869 here ($^{187}Os/^{188}Os$ = 0.1256) and when the exceptionally depleted abyssal peridotites of
870 Harvey et al. (2006) are excluded are almost indistinguishable from each other (abyssal
871 peridotite $^{187}Os/^{188}Os$ = 0.1257; Snow & Reisberg, 1995; Brandon et al., 2000; Liu et al.,
872 2008). Abundances of PGE are also similar in oceanic mantle and SCLM, both in terms of
873 absolute abundances and co-variation of paired IPGE and PPGE in bulk-rock peridotite (Fig
874 9b) and sulfides derived from them (Fig 9c; cf. Luguet et al., 2001, 2003, 2004) so during
875 melt depletion of both these types of peridotite the redistribution of PGE as a result of sulfide
876 mobility should be comparable. However, caution should be exercised in the choice of
877 material used where for example high S abundances could be the result of large quantities of
878 metasomatic sulfide, in texturally complex peridotites, or where bulk-rock PGE abundances
879 materially differ from those of abyssal peridotites.

880 The possible contribution of PGE from sources other than peridotite-sourced sulfides
881 should also be considered. Many EM-basalts, and OIB in general, are considered to be the
882 product of mixed-source melting with varying proportions being derived from pyroxenite and
883 peridotite (e.g. Hirschmann & Stolper, 1996; Sobolev et al., 2005; 2007). While pyroxenites
884 also contain a significant sulfide fraction it has been demonstrated that in all cases, sulfides

recovered from pyroxenite xenoliths (e.g. Wang et al., 2009; Sen et al., 2010) and non-xenolithic pyroxenites (e.g. van Acken et al., 2010) contain 1-3 orders of magnitude less PGE than their peridotitic counterparts. Thus it would seem unlikely that even in instances where the production of basaltic melt is dominated by the melting of pyroxenite, the contribution to the basalt PGE budget, and hence Os isotope systematics, will be quickly overprinted by the contribution from peridotite hosted sulfide. A model that accounts for the combined contributions of sulfide from mixed source melting has been proposed by Luguet et al. (2008). Their model suggests that during the melting of a pyroxenite – peridotite source the early melting of pyroxenite results in reaction with the peridotite wall-rock (e.g. Yaxley and Green 1998) creating a source rock containing sulfides from both peridotite and pyroxenite. This reacted wallrock then provides the source for low solidus metasomatic sulfides which are readily incorporated into the basaltic melt; the overall PGE signature being dominated by the contribution from the peridotite source rock. Luguet et al. (2008) also go on to speculate about the possible contribution to basalt PGE and $^{187}Os/^{188}Os$ systematics from refractory alloy phases. However it seems difficult to reconcile the physical and chemical properties of these phases (i.e. refractory, dense, unreactive) with the incorporation and / or redistribution into a basaltic melt. In summary, based upon the relative PGE budgets of peridotite and pyroxenite, combined with the unfavourable physical and chemical properties of PGE-rich alloys, the Os isotope systematics of EM-basalts in particular and OIB in general are most likely controlled by peridotite-hosted sulfides.

6. CONCLUDING REMARKS

Bulk-rock PGE, Re-Os elemental and isotope systematics of peridotites, and consequently OIB, including EM-basalts, are controlled by volumetrically insignificant sulfides. More than one population of sulfides, which have large compositional differences between the populations in terms of major elements, PGE and Re-Os elemental and isotope systematics, are commonly present in peridotite samples. This means that bulk-rock Re-Os isotope systematics of peridotite are often merely the aggregate signatures of two populations of sulfide, produced at different times and under different conditions, thus rendering bulk-rock Re-Os isotope geochronology extremely difficult to interpret in all but the most straightforward of examples.

The textural characteristics of the two populations of sulfide govern their behaviour during partial melting; interstitial, metasomatic sulfides being liberated from their peridotite host during the early stages of partial melting, whereas sulfides enclosed within silicate grains only becoming exposed to the generated melt as their host grains themselves start to contribute to the production of basalt. The wide range of mantle sulfide compositions present even within a single peridotite xenolith or within a small number of xenoliths from a restricted geographical area can easily account for the Os compositional and isotopic range of EM-basalts. There is therefore no need for additional mantle reservoirs to account for the apparent co-variation of lithophile-element based and siderophile-element based isotope systems in the generation of EM-basalts.

ACKNOWLEDGEMENTS

We would like to thank John Watson for assistance with the XRF measurements and Andy Tindle for his help with the electron microprobe at The Open University. Funding for this research was provided by NERC grant NER/A/S/2001/00538 which has allowed J.H. to undertake the isotope measurements presented here.

957 # REFERENCES

958

959 Ackerman, L., Walker, R.J., Puchtel, I.S., Pitcher, L., Jelnek, E., Strnad, L. (2009) Effects of
960 melt percolation on highly siderophile elements and Os isotopes in subcontinental
961 lithospheric mantle: A study of the upper mantle profile beneath Central Europe. *Geochim. Cosmochim. Acta* **73**, 2400-2414.

963

964 Alard, O., Griffin, W.L., Pearson, N.J., Lorand, J.-P., O'Reilly, S.Y. (2002) New insights into
965 the Re-Os systematics of sub-continental lithospheric mantle from in-situ analysis of
966 sulphides. *Earth Planet. Sci. Lett.* **203**, 651-663.

967

968 Alard, O., Luguet, A., Pearson, N.J., Griffin, W.L., Lorand, J.-P., Gannoun, A., Burton,
969 K.W., O'Reilly, S.Y. (2005) In-situ Os isotopes in abyssal peridotites bridge the isotopic
970 gap between MORBs and their source mantle. *Nature* **436**, 1005-1008.

971

972 Allègre, C.J., Turcotte, D.L. (1986) Implications of a two-component marble cake mantle.
973 *Nature* **323**, 123-127.

974

975 Aulbach, S., Griffin, W.F., Pearson, N.J., O'Reilly, S.Y., Kivi, K., Doyle, B.J. (2004) Mantle
976 formation and evolution, Slave Craton: constraints from HSE abundances and Re-Os
977 isotope systematics of sulphide inclusions in mantle xenocrysts. *Chem. Geol.* **208**, 61-88.

978

979 Ballhaus, C., Sylvester, P. (1999) Noble metals enrichment processes in the Merensky Reef,
980 Bushveld Complex. *J. Petrol.* **41**, 546-561.

981

982 Ballhaus, C., Bockrath, C., Wohlgemuth-Ueberwasser, C., Laurenz, V., Berndt, J., (2006)
983 Fractionation of the noble metals by physical processes. *Contrib. Mineral. Petrol.* **152**,
984 667–684.
985
986 Basaltic Volcanism Study Project (1981). *Basalt volcanism on the terrestrial planets.*
987 Pergamon Press Inc, New York, 1286 pp.
988
989 Becker, H., Horan, M.F., Walker, R.J., Gao, S., Lorand, J.-P., Rudnick, R.L. (2006) Highly
990 siderophile element composition of the Earth's primitive upper mantle: Constraints from
991 new data on peridotite massifs and xenoliths. *Geochim. Cosmochim. Acta* **70**, 4528-4550.
992
993 Bennett, V.C., East, T.M., Norman, M.D. (1996) Two mantle plume components in Hawaiian
994 picrites inferred from correlated Os-Pb isotopes. *Nature* **381**, 67-83.
995
996 Birck, J.-L., Roy-Barman, M., Capmas F. (1997) Re–Os isotopic measurements at the
997 femtomole level in natural samples. *Geostand. Newslett.* **20**(1), 19–27.
998
999 Bockrath, C., Ballhaus, C., Holzheid, A. (2004) A mechanism for the fractionation of highly
1000 siderophile elements during mantle melting. *Science* **305**, 1951-1953.
1001
1002 Brandon, A.D., Becker, H., Carlson, R.W., Shirey, S.B. (1999) Isotopic constraints on
1003 timescales and mechanisms of slab material transport in the mantle wedge: evidence for
1004 the regional uniformity of CO_2 and H_2O rich fluids in lithospheric mantle. *Earth Planet.*
1005 *Sci. Lett.* **160**, 387-407.
1006

1007 Brandon, A.D., Snow, J.E., Walker, R.J., Morgan, J.W., Mock, T.D. (2000). $^{190}Pt - ^{186}Os$ and
1008 ^{187}Re-^{187}Os systematics of abyssal peridotites. *Earth Planet. Sci. Lett*. **177**, 319-355.
1009
1010 Brandon, A.D., Graham, D.W., Waight, T., Gautason, B. (2007) ^{186}Os and ^{187}Os enrichments
1011 and high $^{3}He/^{4}He$ sources in the Earth's mantle: evidence from Icelandic picrites.
1012 *Geochim. Cosmochim. Acta* **71**, 4570-4591.
1013
1014 Brenan, J.M., McDonough, W.F., Dalpé, C. (2003) Experimental constraints on the
1015 partitioning of rhenium and some platinum-group elements between olivine and silicate
1016 melt. *Earth Planet. Sci. Lett.* **212**, 135-150.
1017
1018 Brenan, J.M., McDonough, W.F., Ash, R. (2005) An experimental study of the solubility and
1019 partitioning of iridium, osmium and gold between olivine and silicate melt. *Earth Planet.*
1020 *Sci. Lett.* **237**, 855-872.
1021
1022 Burnham, O.M., Rogers, N.W., Pearson, D.G., van Calsteren, P., Hawkesworth, C.J. (1998)
1023 The petrogenesis of the eastern Pyrrenian peridotites: An integrated study of their whole-
1024 rock geochemistry and Re-Os isotope composition. *Geochim. Cosmochim. Acta* **62,** 2293-
1025 2310.
1026
1027 Burton, K.W., Schiano, P., Birck, J.-L., Allègre, C.J. (1999) Osmium isotope disequilibrium
1028 between mantle minerals in a spinel-lherzolite. *Earth Planet. Sci. Lett.* **172**, 311-322.
1029

1030 Burton, K.W., Gannoun, A., Birck, J-L., Allegre, C.J., Schiano, P., Clocchiatti, R., Alard, O.
1031 (2002) The compatibility of rhenium and osmium in natural olivine and their behaviour
1032 during melting and basalt genesis. *Earth Planet. Sci. Lett*. **198**, 63-76.
1033
1034 Bussod, G.Y.A. (1981) Thermal and kinematic history of mantle xenoliths from Kilbourne
1035 Hole, New Mexico. *(MSc thesis).* University of Washington, Seattle. 72pp.
1036
1037 Bussod, G.Y.A., Irving, A.J. (1981) Thermal and rheological history of the upper mantle
1038 beneath the southern Rio Grande Rift: evidence from Kilbourne Hole xenoliths. In: *Papers*
1039 *presented to the conference on the proceedings of planetary rifting.* Lunar and Planetary
1040 Institute. Contribution No. **457**, 145-148.
1041
1042 Bussod, G.Y.A., Williams, D.R. (1991) Thermal and kinematic model of the southern Rio
1043 Grande rift: inferences from crustal and mantle xenoliths from Kilbourne Hole, New
1044 Mexico. *Tectonophysics* **197**, 373-389.
1045
1046 Cabri, L. (1992) The distribution of trace metals in minerals and mineral products, *Mineral.*
1047 *Mag*. **56**, 289-308.
1048
1049 Carlson R.W., Irving A.J. (1994) Depletion and enrichment history of sub-continental
1050 lithospheric mantle: an Os, Sr, Nd and Pb isotopic study of ultramafic xenoliths from the
1051 northwestern Wyoming craton. *Earth Planet. Sci. Lett.* **126**, 457–472.
1052
1053 Carter, J.L. (1965). The origin of olivine bombs and related inclusions in basalts (*PhD*
1054 *thesis*). Rice University, Houston. 275pp.

Chu, Z.-Y., Wu, F.-Y., Walker, R.J., Rudnick, R.L., Pitcher, L., Puchtel, I.S., Yang, Y.-H., Wilde, S.A. (2009) Temporal evolution of the lithsopheric mantle beneath the East North China craton. *J. Petrol.* **50**, 1857-1898.

Class, C., Goldstein, S.L., Shirey, S.B. (2009) Osmium isotopes in Grande Comore lavas: a new extreme among a spectrum of EM-type mantle endmembers. *Earth Planet. Sci. Lett.* **284**, 219-227.

Cohen, A.S., Waters, F.G. (1996) Separation of osmium from geological materials by solvent extraction for analysis by TIMS. *Anal. Chim. Acta* **332** 269–275.

Coisy P., Nicolas A. (1978) Regional structure and geodynamics of the upper mantle beneath the Massif Central. *Nature* **274**, 429–432.

Creaser, R.A., Papanastassiou, D.A., Wasserburg, G.J. (1991) Negative thermal ion mass spectrometry of osmium, rhenium, and iridium. *Geochim. Cosmochim. Acta* **55**, 397–401.

Dale, C.W., Luguet, A., Macpherson, C.G., Pearson, D.G., Hickey-Vargas, R. (2008) Extreme platinum-group element fractionation and variable Os isotope compositions in Philippine Sea Plate basalts: tracing mantle source heterogeneity. *Chem. Geol.* **248**, 213–238.

1078 Day, J.M.D., Pearson, D.G., MacPherson, C.G., Lowry, D., Carracedo, J.C. (2009)
1079 Pyroxenite-rich mantle formed by recycled oceanic lithosphere: oxygen-osmium isotopic
1080 evidence from Canary Island lavas. *Geology* **37**, 555-558.
1081
1082 Debaille, V., Troennes, R.G., Brandon, A.D., Waight, T.E., Graham, D.W., Lee, C.-T.A
1083 (2009) Primitive off rift basalts from Iceland and Jan Mayen: osmium isotopic evidence
1084 for a mantle source containing enriched sub-continental lithosphere. *Geochim.*
1085 *Cosmochim. Acta* **73**, 3423-3449.
1086
1087 Dromgoole, E.L., Pasteris, J.D. (1987) Interpretation of the sulphide assemblages in a suite of
1088 xenoliths from Kilbourne Hole, New Mexico. *Geol. Soc. Am. Spec. Pap.* **215**, 25–46.
1089
1090 Eggler D. H., Lorand J.-P. (1993) Mantle sulfide oxybarometry. *Geochim. Cosmochim. Acta*
1091 **57**, 2213–2222.
1092
1093 Eisele, J., Sharma, M., Galer, S.J.G., Blichert-Toft, J., Devey, C.W., Hofmann, A.W. (2002)
1094 The role of sediment recycling in EM-1 inferred from Os, Pb, Hf, Nd, Sr isotope and trace
1095 element systematics of the Pitcairn hotspot. *Earth Planet. Sci. Lett.* **196**, 197-212.
1096
1097 Escrig, S., Schiano, P., Schilling, J.-G., Allègre, C.J. (2005) Rhenium-osmium isotope
1098 systematics in MORB from the Southern Mid-Atlantic Ridge (40^{o}-50^{o}S). *Earth Planet.*
1099 *Sci. Lett.* **235**, 528-548.
1100

1101 Fleet, M.E., Stone, W.E., Crocket, J.H. (1991) Partitioning of palladium, iridium, and
1102 platinum between sulphide liquid and basalt melt: Effects of melt composition,
1103 concentration and oxygen fugacity. *Geochim. Cosmochim. Acta* **55**, 2545-2554.
1104
1105 Fleet, M.E., Crocket, J.H., Stone, W.E. (1996) Partitioning of platinum group elements (Os,
1106 Ir, Ru, Pt, Pd) and gold between sulphide liquid and basalt melt. *Geochim. Cosmochim.*
1107 *Acta* **60**, 2397-2412.
1108
1109 Frey F.A., Green, D.H. (1974) The mineralogy, geochemistry and origin of lherzolite
1110 inclusions in Victorian basanites. *Geochim. Cosmochim. Acta* **38**, 1023–1059.
1111
1112 Gaffney, A.M., Nelson, B.K., Reisberg, L., Eiler, J.M. (2005) Oxygen-osmium isotope
1113 systematics of West Maui lavas: a record of shallow-level magmatic processes. *Earth*
1114 *Planet. Sci. Lett.* **239**, 122-139.
1115
1116 Galer, S.J.G., O'Nions, R.K. (1989) Chemical and isotopic studies of ultramafic inclusions
1117 from the San Carlos Volcanic Field, Arizona: a bearing on their petrogenesis. *J. Petrol.* **30**,
1118 1033–1064.
1119
1120 Gannoun, A., Burton, K.W., Thomas, L.E., Parkinson, I.J., van Calsteren, P.W., Schiano, P.
1121 (2004) Osmium isotope heterogeneity in the constituent phases of mid-ocean ridge basalts.
1122 *Science* **303**, 70-72.
1123

Gannoun, A., Burton, K.W., Parkinson, I.J., Alard, O., Schiano, P., Thomas, L.E. (2007) The scale and origin of the osmium isotope variations in mid-ocean ridge basalts. *Earth Planet. Sci. Lett.* **259**, 541-556.

Griffin, W.L., O'Reilly, S.Y., Abe, N., Aulbach, S., Davies, R.M., Pearson, N.J., Doyle, B.J., Kivi, K. (2003) The origin and evolution of Archean lithospheric mantle. *J. PreCam. Res.* **127**, 19-41.

Griffin, W.L., Graham, S., O'Reilly, S.Y., Pearson, N.J. (2004) Lithosphere evolution beneath the Kaapvaal craton: Re-Os systematics of sulphides in mantle derived peridotites. *Chem. Geol.* **208**, 89-118.

Hammond, S.J., Yoshikawa, M., Harvey, J., Burton, K.W. (2010). Multiple metasomatic events recorded in Kilbourne Hole peridotite xenoliths: the relative contribution of host basalt interaction vs. silicate metasomatic glass. *AGU Fall 2010 meeting*, abstract **V23b**, 2413.

Handler, M.R., Bennett, V.C. (1999) Behaviour of platinum-group elements in the sub-continental mantle of eastern Australia during variable metasomatism and melt depletion. *Geochim. Cosmochim. Acta* **63**, 3597-3618.

Hanghøj, K., Kelemen, P.B., Hassler, D., Godard, M. (2010) Composition and genesis of depleted mantle peridotites from the Wadi-Tayan Massif, Oman ophiolite: major and trace element geochemistry, and Os isotope and PGE systematics. *J. Petrol.* **51**, 201-227.

1149 Hart, S.R. (1988) Heterogeneous mantle domains: signatures, genesis and mixing
1150 chronologies. *Earth Planet. Sci. Lett.* **90**, 273-296.
1151
1152 Hart, S.R., Ravizza, G. (1996) Os partitioning between phases in lherzolite and basalt. *In*
1153 *Earth Processes: Reading the Isotopic Code (eds. Basu, A. and Hart, S. R.) AGU,*
1154 *Washington, Geophys. Mon*. **95**, 123–134.
1155
1156 Harvey, J., Gannoun, A., Burton, K.W., Rogers, N.W., Alard, O., Parkinson, I.J. (2006)
1157 Ancient melt extraction from the oceanic upper mantle revealed by Re-Os isotopes from
1158 the Mid-Atlantic Ridge. *Earth Planet. Sci. Lett.* **244**, 606-621.
1159
1160 Harvey, J., Gannoun, A., Burton, K.W., Rogers, N.W., Schiano, P., Alard, O. (2010)
1161 Unravelling the effects of melt depletion and secondary infiltration on mantle Re–Os
1162 isotopes beneath the French Massif Central. *Geochim. Cosmochim. Acta* **74**, 293-320.
1163
1164 Hauri, E.H., Lassiter, J.C., DePaulo, D.J. (1996) Osmium isotope systematics of drilled lavas
1165 from Mauna Loa, Hawaii. *J. Geophys. Res.* **B101**, 11793-11806.
1166
1167 Hauri, E.H., Kurz, M.D. (1997) Melt migration and mantle chromatography 2: A time-series
1168 Os-isotope study of Mauna Loa volcano, Hawaii. *Earth Planet. Sci. Lett.* **153**, 21-36.
1169
1170 Hauri E.H., Hart S.R. (1997) Rhenium abundances and systematics in oceanic basalts. *Chem.*
1171 *Geol.* **139**, 185–205.
1172

1173 Hirschmann, M.M., Stolper, E.M. (1996) A possible role for garnet pyroxenite in the origin
1174 of "garnet signature" in MORB. *Contrib. Mineral. Petrol.* **124**, 185-208.
1175
1176 Hoffer, J.M. (1976) The Potrillo basalt field, south-central New Mexico. In: Cenozoic
1177 volcanism in southwestern New Mexico. (Eds) Elston, W., Northrop, S.A. *New Mexico*
1178 *Geol. Soc. Special Pub.* **5**, 89-92.
1179
1180 Hofmann, A.W. (1997) Mantle geochemistry: the message from oceanic volcanism. *Nature*,
1181 **385**, 219-229.
1182
1183 Holzheid, A. (2010) Separation of sufide melt droplets in sulphur saturated silicate liquids.
1184 *Chem. Geol.* **274**, 127-135.
1185
1186 Horan, M.F., Walker, R.J., Morgan, J.W., Grossman, J.N., Rubin, A.E. (2003) Highly
1187 siderophile elements in chondrites. *Chem. Geol.* **196**, 27-42.
1188
1189 Hsieh, J.-C., Vkach, K.C., Chang, Y.A. (1987) The Fe–Ni–S system: I. A thermodynamic
1190 analysis of the phase equilibria calculation of the phase diagram from 1173 to 1623 K.
1191 *High Temp. Sci.* **23,** 17–38.
1192
1193 Ionov, D.A., Dupuy, C., O'Reilly, S.Y., Kopylova, M.G., Genschaft Y.S. (1993) Carbonated
1194 peridotite xenoliths from Spitzbergen: implications for the trace element signature of
1195 mantle carbonate metasomatism. *Earth Planet. Sci. Lett.* **119**, 283–297.
1196

1197 Ireland, T.J., Walker, R.J., Garcia, M.O. (2009) Highly siderophile element and ^{187}Os isotope
1198 systematics of Hawaiian picrites: implications for parental melt composition and source
1199 heterogeneity. *Chem. Geol.* **260**, 112-128.
1200
1201 Irving, A.J. (1979) Kilbourne Hole spinel lherzolites: samples of multiply depleted, enriched
1202 and deformed mantle. *Abstr. EOS transactions, American Geophysical Union* **60**, 418.
1203
1204 Irving, A.J. (1980) Petrology and geochemistry of composite ultramafic xenoliths in alkali
1205 basalts and implications for magmatic processes in the mantle. *Am. J. Sci.* **280-A**, 389–
1206 426.
1207
1208 Ivanov, A.V., Palesskii, S.V., Demonterova, E.I., Nikolaeva, I.V., Ashchepkov, I.V.,
1209 Rasskazov, S.V. (2008) Platinum-group elements and rhenium in mantle xenoliths from
1210 the East Sayan volcanic field (Siberia, Russia): evaluation of melt extraction and
1211 refertilization processes in lithospheric mantle of the Tuva-Mongolian Massif. *Terra*
1212 *Nova* **20**, 504-511.
1213
1214 Jagoutz, E., Palme, H., Blum, H., Cendales, M., Dreibus, G., Spettel, B., Lorenz, V., Wänke,
1215 H. (1979) The abundances of major, minor and trace elements in the Earth's mantle as
1216 derived from primitive ultramafic nodules. Proceedings of 10th LPSC. *Geochim.*
1217 *Cosmochim. Acta Supplement* **10**, 2031–2051.
1218
1219 Jamais, M., Lassiter, J.C., Brügmann, G.E. (2008) PGE and Os-isotopic variations in lavas
1220 from Kohala volcano, Hawaii: constraints on PGE behaviour and melt/crust interaction.
1221 *Chem. Geol.* **250**, 16-28.

Kil, Y., Wendlandt, R.F. (2004) Pressure and temperature evolution of upper mantle under the Rio Grande rift. *Contrib. Miner. Petrol.* **148,** 2665-2680.

Kuno H., Aoki, K. (1970) Chemistry of ultramafic nodules and their bearing on the origin of basaltic magmas. *Phys. Earth Planet. Interiors* **3**, 273–301.

Lassiter, J.C., Hauri, E.H. (1998) Osmium isotope variations in Hawaiian lavas: evidence for recycled oceanic lithosphere in the Hawaiian plume. *Earth Planet. Sci. Lett.* **164**, 483-496.

Lassiter, J.C., Hauri, E. H., Reiners, P.W., Garcia, M.O. (2000) Generation of Hawaiian post-erosional lavas by melting of a mixed lherzolite/pyroxenite source. *Earth Planet. Sci. Lett.* **178**, 269-284.

Lassiter, J.C. (2003) Rhenium volatility in sub-aerial lavas: constraints from sub-aerial and submarine portions of the HSDP-2 Mauna Kea drillcore. *Earth Planet. Sci. Lett.* **214**, 311-325.

Liu, C.-Z., Snow, J.E., Hellebrand, E., Brügmann, G., von der Handt, A., Büchl, A., Hofmann, A.W. (2008) Ancient, highly heterogeneous mantle beneath Gakkel Ridge, Arctic Ocean. *Nature* **452**, 311-316.

Lorand, J.-P., Alard, O. (2001) Platinum-group element abundances in the upper mantle: New constraints from in-situ and whole-rock analyses of Massif Central xenoliths (France). *Geochim. Cosmochim. Acta* **65**, 2789-2806.

Lorand, J.-P., Alard, O., Luguet, A., Keays, R.R. (2003) Sulphur and selenium systematics of the sub-continental lithospheric mantle: Inferences from the Massif Central xenolith suite (France). *Geochim. Cosmochim. Acta* **67**, 4137-4151.

Luck J.M., Allègre, C.J. (1983) ^{187}Re-^{187}Os systematics in meteorites and cosmochemical consequences. *Nature* **302**,130–32.

Luguet, A., Alard, O., Lorand, J.-P., Pearson, N.J., Ryan, C., O'Reilly, S.Y. (2001) Laser ablation microprobe (LAM)-ICPMS reveals the highly siderophile element geochemistry of the oceanic mantle. *Earth Planet. Sci. Lett.* **189**, 285-294.

Luguet, A., Lorand, J.-P., Seyler, M. (2003) Sulphide petrology and highly siderophile element geochemistry of abyssal peridotites: a coupled study of from the Kane Fracture Zone (45°W, 23°20′N, MARK Area, Atlantic Ocean). *Geochim. Cosmochim. Acta* **67**, 1553-1570.

Luguet, A., Lorand, J.-P., Alard, O., Cottin, J.-Y. (2004) A multi-technique study of platinum group element systematic in some Ligurian ophiolitic peridotites, Italy. *Chem. Geol.* **208**, 175-194.

Luguet, A., Pearson, D.G., Nowell, G.M., Dreher, S.T., Coggan, J.A., Spetsius, Z.V., Parman, S.W. (2008) Enriched Pt-Re-Os isotope systematics in plume lavas explained by metasomatic sulphides. *Science* **319**, 453-456.

1272 Mackovicky, M., Mackovicky, E., Rose-Hansen, J. (1986) Experimental studies on the
1273 solubility and distribution of platinum group elements in base-metal sulfides in platinum
1274 deposits, in: Metallogeny of Basic and Ultrabasic Rocks. Eds: Gallagher, M.J., Ixer, R.A.,
1275 Neary, C.R., Prichard, H.M., *Inst. Mineral. Metall*., pp. 415-425.
1276
1277 Mallmann G., O'Neill H.St.C. (2007) The effect of oxygen fugacity on the partitioning of
1278 rhenium between crystals and silicate melt during mantle melting. *Geochimica et*
1279 *Cosmochimica Acta* **71**, 2837-2857.
1280
1281 Manga, M. (1996) Mixing of heterogeneities in the mantle: effect of viscosity differences.
1282 *Geophys. Res. Lett.* **23** 403–406.
1283
1284 Martin, C.E., Carlson, R.W., Frey, F.A., Chen, C.-Y. (1994) Os-isotopic variation in basalts
1285 from Haleakala volcano, Maui, Hawaii: a record of magmatic processes in oceanic mantle
1286 and crust. *Earth Planet. Sci. Lett.* **128**, 287-301.
1287
1288 Marchesi, C., Griffin, W.F., Garrido, C.J., Bodinier, J.-L., O'Reilly, S.Y., Pearson, N.J.
1289 (2009) Persistence of mantle lithospheric Re-Os isotopic signature during
1290 asthenospherization of the sub-continental lithospheric mantle: insights from in-situ
1291 isotopic analyses of sulphides from the Ronda peridotite (Southern Spain). *Contrib.*
1292 *Mineral. Petrol.* **159**, 315-330.
1293
1294 Meisel, T., Walker, R.J., Morgan, J.W. (1996) The osmium isotopic composition of the
1295 Earth's upper mantle. *Nature* **383**, 517-520.
1296

1297 Meisel, T., Walker, R.J., Irving, A.J., Lorand, J.P. (2001) Osmium isotopic composition of
1298 mantle xenoliths: a global perspective. *Geochim. Cosmochim. Acta* **65**, 1311-1323.
1299
1300 Meisel, T., Reisberg, L., Moser, J., Carignan, J., Melcher, F., Brügmann, G.E. (2003) Re–Os
1301 systematics of UB–N, a serpentinised peridotite reference material. *Chem. Geol.* **201**, 161–
1302 179.
1303
1304 Meisel, T., Moser, J., Kettisch, P. (2008) Determination of osmium and other platinum group
1305 elements in chromitites by acid digestion and ICPMS. Department of General and
1306 Analytical Chemistry, University of Leoben, Leoben, p. 1.
1307
1308 Morgan, J.W. (1986) Ultramafic xenoliths: clues to Earths late accretionary history. *J.*
1309 *Geophys. Res.* **91**, 12375-12387.
1310
1311 Mungall, J.E., Su, S. (2005) Interfacial tension between magmatic sulphide and silicate
1312 liquids: constraints on kinetics of sulphide liquation and sulphide migration through
1313 silicate rocks. *Earth Planet. Sci. Lett.* **274**, 127-135.
1314
1315 O'Neil, H. St. C. (1991) The origin of the moon and the early history of the Earth – a
1316 chemical model: Part 2 The Earth. *Geochim. Cosmochim. Acta* **55**, 1159-1172.
1317
1318 Pearson, D.G., Shirey, S.B., Carlson, R.W., Boyd, F.R., Pokhilenko, N.P., Shimizu, N.
1319 (1995) Re-Os, Sm-Nd and Rb-Sr isotope evidence for thick Archean lithospheric mantle
1320 beneath the Siberian craton modified by multistage metasomatism. *Geochim. Cosmochim.*
1321 *Acta* **59**, 959-977.

Pearson, D.G., Shirey, S.B., Harris, J.W., Carlson, R.W. (1998) Sulphide inclusions in diamonds from the Koffiefontein kimberlite, South Africa: constraints on diamond ages and mantle Re-Os systematics. *Earth Planet. Sci. Lett.* **160**, 311-326.

Pearson, D.G. (1999) The age of continental roots. *Lithos* **48**, 171-194.

Pearson, D.G., Woodland, S.J. (2000) Carius tube digestion and solvent extraction/ion exchange separation for the analysis of PGEs (Os, Ir, Pt, Pd, Ru) and Re–Os isotopes in geological samples by isotope dilution ICP-mass spectrometry. *Chem. Geol.* **165**, 87–107.

Pearson, D.G., Irvine, G.J., Ionov, D.A., Boyd, F.R., Dreibus, G.E. (2004) Re–Os isotope systematics and platinum group element fractionation during mantle melt extraction: a study of massif and xenolith peridotite suites. *Chem. Geol.* **208**, 29–59.

Pearson, N.J., Alard, O., Griffin, W.L., Jackson, S.E., O'Reilly, S.Y. (2002) In situ measurement of Re-Os isotopes in mantle sulfides by laser-ablation multi-collector inductively coupled plasma mass spectrometry: Analytical methods and preliminary results. *Geochim. Cosmochim. Acta* **66**, 1037-1050.

Pegram B.J., Allègre, C.J. (1992) Osmium isotopic compositions from oceanic basalts. *Earth Planet. Sci. Lett.* **111**, 59–68.

1345 Pitcher, L., Heltz, R.T., Walker, R.W., Piccoli, P. (2009) Fractionation of the platinum-group
1346 elements and Re during crystallization of basalts in Kilauea Iki Lava Lake, Hawaii. *Chem.*
1347 *Geol.* **260**, 196–210.
1348
1349 Qi, L., Zhou, M.-F. (2008) Platinum-group element and Sr-Nd-Os isotope geochemistry of
1350 Permian Emeishan flood basalts, in Guizhou Province, SW China. *Chem. Geol* **248**, 83-
1351 103.
1352
1353 Reid, J.B., Woods, G.A. (1978) Oceanic mantle beneath the southern Rio Grande Rift. *Earth*
1354 *Planet. Sci. Lett.* **41**, 303-316.
1355
1356 Reisberg, L., Zindler, A., Marcantonio, F., White, W., Wyman, D., Weaver, B. (1993) Os
1357 isotope systematics in ocean island basalts. *Earth Planet. Sci. Lett.* **120**, 149-167.
1358
1359 Reisberg, L., Lorand, J.-P. (1995) Longevity of sub-continental mantle lithosphere from
1360 osmium isotope systematics in orogenic peridotite massifs. *Nature*, **376**, 159-162.
1361
1362 Reisberg, L., Zhi, X., Lorand, J.-P., Wagner, C., Peng, Z., Zimmermann, C. (2005) Re-Os
1363 and S systematics of spinel peridotite xenoliths from east central China: Evidence for
1364 contrasting effects of melt percolation. *Earth Planet. Sci. Lett.* **239,** 286-308.
1365
1366 Righter, K., Chesley, J.T., Geist, D., Ruiz, J. (1998) Behaviour of Re during magma
1367 fractionation: an example from Volcan Alcedo, Galapagos. *J. Petrol.* **39**, 785-795.
1368

1369 Righter K., Campbell A.J., Humayun M., Hervig R.L. (2004) Partitioning of Ru, Rh, Pd, Re,
1370 Ir, and Au between Cr-bearing spinel, olivine, pyroxene and silicate melts. *Geochim.*
1371 *Cosmochim. Acta* **68**, 867–880.
1372
1373 Roden, M.F., Irving, A.J., Murthy, V.R. (1988) Isotopic and trace element composition of
1374 the upper mantle beneath a young continental rift: Results from Kilbourne Hole, New
1375 Mexico. *Geochim. Cosmochim. Acta* **52**, 461-476.
1376
1377 Ross, C.S., Foster, D.M., Myers, A.T. (1954) Origin of dunites and olivine rich inclusions in
1378 basaltic rocks. *Am. Mineral.* **39**, 693–737.
1379
1380 Roy-Barman, M, Allègre C.J. (1995) $^{187}Os/^{186}Os$ in oceanic island basalts: tracing oceanic
1381 crust recycling in the mantle. *Earth Planet. Sci. Lett.* **129**, 145-161.
1382
1383 Rudnick, R.L., Walker, R.J. (2009) Interpreting ages from Re–Os isotopes in peridotites.
1384 *Lithos* **112S**, 1083-1095.
1385
1386 Sen, I.S., Bizimis, M., Sen, G. (2010) Geochemistry of sulphides in Hawaiian garnet
1387 pyroxenite xenoliths: Implications for highly siderophile elements in the oceanic mantle.
1388 *Chem. Geol.* **273**, 180-192.
1389
1390 Shirey, S.B., Walker, R.J. (1995) Carius tube digestion for low blank rhenium–osmium
1391 analysis. *Anal. Chem.* **34**, 2134–2141.
1392

1393 Shirey, S.B., Walker, R.J. (1998) The Re-Os isotope system in cosmochemistry and high
1394 temperature geochemistry. *Annu. Rev. Earth Planet. Sci.* **26**, 423-500.
1395
1396 Skovgaard, A.C., Storey, M., Baker, J.A., Blusztajn, J. (2001) Osmium-oxygen isotopic
1397 evidence for a recycled and strongly depleted component in the Iceland mantle plume.
1398 *Earth Planet. Sci. Lett.* **194**, 259-275.
1399
1400 Snow, J.E., Reisberg, L. (1995). Os isotopic systematics of the MORB mantle: results from
1401 altered abyssal peridotites. *Earth Planet. Sci. Lett.* **133**, 411-421.
1402
1403 Sobolev, A.V., Hofmann, A.W., Sobolev, S.V., Nikokosian, I.K. (2005) An olivine-free
1404 mantle source of Hawaiian shield basalts. *Nature* **434**, 590-597.
1405
1406 Sobolev, A.V., Hofmann, A.W., Kuzmin, D.V., Yaxley, G.M., Arndt, N.T., Chung, S.-L.,
1407 Danyushevsky, L.V., Elliott, T., Frey, F.A., Garcia, M.O., Gurenko, A.A., Kamenetsky,
1408 V.S., Kerr, A.C., Krivolutskaya, N.A., Matvienkov, V.V., Nikogosian, I.K., Rocholl, A.,
1409 Sigurdsson, I.A., Sushchevskaya, N.M., Teklay, M. (2007) The amount of recycled crust
1410 in mantle-derived melts. *Science* **316**, 412-417.
1411
1412 Stern, C.R., Saul, S., Skewes, M.A., Futa., K. (1989) Garnet peridotite xenoliths from the
1413 Pali-Aike alkali basalts of southern-most South America. In: *Kimberlites and related*
1414 *rocks,* (Ed: Ross, J.) *Geol. Soc. Austral. Spec. Publ*. **14**. Blackwell, Perth. Vol 2, 735-744.
1415
1416 Stosch H.G., Seck H.A. (1980) Geochemistry and mineralogy of two spinel peridotite suites
1417 from Dreiser Weiher, West Germany. *Geochim. Cosmochim. Acta* **44**, 457–470.

1418

1419 Stracke, A., Hofmann, A.W., Hart, S.R. (2005) FOZO, HIMU and the rest of the mantle zoo.
1420 *Geochem., Geophys., Geosys*. **6**, doi:10.1029/2004GC000824.

1421

1422 Sun, W., Bennett, V.C., Kamenetsky, V.S. (2004) The mechanism of Re enrichment in arc
1423 lavas: evidence from Lau basin basaltic glasses and primitive melt inclusions. *Earth*
1424 *Planet. Sci. Lett*. **222**, 101-114.

1425

1426 Tarantola A., Valette B. (1982) Generalized non-linear inverse problems solved using the
1427 least squares criterion. *Rev. Geophys. Space Phys.* **20**, 219–232.

1428

1429 Thompson, R.N., Ottley, C.J., Smith, P.M., Pearson, D.G., Dickin, A.P., Morrison, M.A.,
1430 Leat, P.T., Gibson, S.A. (2005) Source of the Quaternary alkalic basalts, picrites and
1431 basanites of the Potrillo volcanic field, New Mexico, USA: Lithosphere or convecting
1432 mantle? *J.Petrol.* **46,** 1603-1643**.**

1433

1434 van Acken, D., Becker, H., Walker, R.J., McDonough, W.F., Wombacher, F., Ash, R.D.,
1435 Piccoli, P.M. (2010) Formation of pyroxenite layers in the Totalp ultramafic massif (Swiss
1436 Alps) - Insights from highly siderophile elements and Os isotopes. *Geochimica et*
1437 *Cosmochimica Acta* **74**, 661-683.

1438

1439 Volkening J., Walczyk T., Heumann K. (1991) Os isotope ratio determinations by negative
1440 thermal ionisation mass spectrometry. *Int. J. Mass Spectrom. Ion Process.* **105**, 147–159.

1441

1442 Walker, R.J, Morgan J.W. (1989) Rhenium-osmium isotope systematics of carbonaceous

chondrites. *Science* **243**, 519–22.

Wang, K.L., O'Reilly, S.Y., Griffin, W.F., Pearson, N.J., Zhang, M. (2009) Sulphides in peridotite xenoliths from Penghu Islands, Taiwan: melt percolation, PGE fractionation and the lithospheric evolution of the South China block. *Geochim. Cosmochim. Acta* **73**, 4531-4557.

Widom, E., Hoernle, K.A., Shirey, S.B., Schminke, H.-U. (1999) Os isotope systematics in the Canary Islands and Madeira: lithospheric contamination and mantle plume signatures. *J. Petrol.* **40**, 279-296.

Wilshire, H.G., Shervais, J.W. (1975) Al-augite and Cr-diopside ultramafic xenoliths in basaltic rocks from the Western United States. *Phys. Chem. Earth* **9**, 257–272.

Wittig, N., Pearson, D.G., Baker, J.A., Duggen, S., Hoernle, K. (2010) A major element, PGE and Re-Os isotope study of Middle Atlas (Morocco) peridotite xenoliths: Evidence for coupled introduction of metasomatic sulphides and clinopyroxene. *Lithos* **115**, 15-26.

Workman, R.K., Hart, S.R., Jackson, M.G., Regelous, M., Farley, K.A., Blusztajn, J., Kurz, M.D., Staudigel, H. (2004) Recycled metasomatized lithosphere as the origin of the enriched mantle II (EM2) end-member: evidence from the Samoan volcanic chain. *Geochem. Geophys. Geosys.* **5**, (2003GC000623).

Yaxley, G.M., Green, D.H. (1998) Reactions between eclogite and peridotite: mantle refertilisation by subduction of oceanic crust. *Schweiz Mineral. Petrog. Mitt.* **78**, 243.

Zindler, A., Hart, S.R. (1986) Chemical geodynamics. *Ann. Rev. Earth Planet. Sci.* **14**, 493-571.

FIGURE CAPTIONS

Figure 1. Rhenium and osmium elemental abundances of 28 spinel lherzolite xenoliths from Kilbourne Hole (this study) and similar samples from the same locality (Morgan, 1986; Burton et al., 1999; Meisel et al., 2001). All concentrations in parts per billion (ppb). Grey square illustrates estimates for [Os] and [Re] of the primitive upper mantle (PUM) of 3.9 ppb and 0.35 ppb respectively (Becker et al., 2006).

Figure 2. (a) Re-Os isotope evolution diagram for the 28 bulk-rock peridotites from this study (Burton et al., 1999 and Meisel et al., 2001 shown for comparison). Scatter between $^{187}Re/^{188}Os$ and $^{187}Os/^{188}Os$ is particularly high amongst the xenoliths from Kilbourne Hole. The best fit line coincides with a calculated isochron age of 2.3 ± 0.7 Ga, but the relationship cannot be described as convincingly isochronous despite agreement with the ages derived from Sr isotope ratios of Roden et al. (1988) of 2.5 Ga ± 0.2 Ga. (b) "Aluminachron" diagram for same samples as (a). Using an immobile melt depletion index, e.g. bulk-rock aluminium abundance reduces the amount of scatter seen in (a) suggesting a certain degree of Re-mobility. Best fit line of 2.4 Ga passes through composition of PUM (Meisel et al., 2001). Dashed lines – calculated Os isotope ratios for different mantle Re-depletion ages ($T_{RD} = 1/\lambda$ x $\ln\{[(^{187}Os/^{188}Os_{chon} - {}^{187}Os/^{188}Os_{sample})/^{187}Re/^{188}Os_{chon}]+1\}$ (Shirey & Walker, 1998).

Figure 3. Chondrite-normalized platinum-group element concentrations for 5 bulk-rock Kilbourne Hole peridotites (KH03-10, KH03-15, KH03-16, KH03-21 & KH03-24) and the host basalt (CI chondrite values from Horan et al., 2003). Uncertainties (2 σ) calculated from long-term reproducibility of reference material GP13 and from external reproducibility of repeat measurements on separate aliquots of samples from this study.

1515

1516 Figure 4. Major element abundances of 57 sulfides (see Table 3). Two low-Cu populations
1517 (0.08 to 4.68 wt %), defined by either a high or low Fe:Ni ratio, are broadly equivalent to
1518 pentlandite rich and pentlandite poor monosulfide solid solution (MSS) sulfides (Luguet et
1519 al., 2003, 2004). A third population of sulfide, with higher Cu content, is analogous to
1520 chalcopyrite rich sulfides from previous studies (Dromgoole & Pasteris, 1987; Luguet et al.,
1521 2003, 2004). Host basalt sulfide from Burton et al. (1999).

1522

1523 Figure 5. (a) Bulk rock peridotite [Os] vs. bulk rock Os isotope ratios. (b) [Os] and
1524 $^{187}Os/^{188}Os$ of individual sulfides from KH03-15 (n = 7), KH03-16 (n = 7), KH03-21 (n =
1525 10), and KH03-24 (n = 8). Open circles denote interstitial sulfides, closed circles denote
1526 enclosed sulfides. Grey box denotes range of [Os] and $^{187}Os/^{188}Os$ in (a). As in cratonic
1527 mantle sulfides (e.g. Griffin et al., 2004), and other non-cratonic sulfides (e.g. Harvey et al.,
1528 2006; 2010) the most unradiogenic sulfides possess the greatest [Os]. (c) Sulfide [Re] vs.
1529 sulfide [Os] for 7 interstitial and 12 enclosed sulfides from (b). There is no statistically
1530 significant co-variation between these variables, however sulfides with high [Re] tend to
1531 possess low [Os] and c. 50% of the high-[Os] enclosed have lower [Re] than the interstitial
1532 population.

1533

1534 Figure 6. Osmium mass balance for Kilbourne Hole xenoliths. The silicate and oxide phases
1535 (olivine, orthopyroxene, clinopyroxene and spinel) account for less than 5 % of the whole
1536 rock Os budget. Sulfide dominates the Os budget of all of the samples due to exceptionally
1537 high sulfide / silicate partition coefficients for Os (e.g. Fleet et al 1991, 1996). At least two
1538 populations of sulfide exist, in approximately equal modal abundance not exceeding a total of
1539 0.03 modal% (cf. Luguet et al., 2003; 2004), but their respective contribution to the Os mass

balance are not equal. In all samples, enclosed sulfides account for the vast majority of Os while the contribution from interstitial sulfide, in the case of KH03-24, is insignificant, and in KH03-15 and KH03-21 account for 3.5 - 17.5 % respectively of the Os present. The relative contributions of the two sulfide populations in KH03-16 is less clear but is probably dominated by the enclosed population. The contribution of the interstitial component in KH03-16 is calculated to be less than 17.5 % of the total. Relative contributions to the osmium budget were calculated on the basis of the [Os] and $^{187}Os/^{188}Os$ of individual components and the bulk-rock rather than by point counting the two populations of sulfide, which are sparse in thin section.

Figure 7. ^{187}Re-^{187}Os isotope systematics for all mineral components, interstitial and enclosed sulfides and host basalt from KH03-15, KH03-16, KH03-21 & KH03-24. With the exception of KH03-16, all samples show a strong similarity between the ^{187}Re-^{187}Os systematics of enclosed sulfides and the respective bulk-rock. Although no high-[Os] sulfides with particularly unradiogenic ($^{187}Os/^{188}Os < 0.120$) were recovered from KH03-16 a high-[Os], unradiogenic component, i.e. enclosed sulfide, must be present in KH03-16 to complete the Os mass balance (see text & Figure 6).

Figure 8. A simple two-stage model for the generation of EM-basalt Os isotope signatures. Black squares denote Os elemental abundance and isotope signature of EM-basalts worldwide (Martin et al., 1994; Bennett et al., 1996; Hauri & Kurz, 1996; Hauri et al., 1996; Lassiter & Hauri, 1998; Widom et al., 1999; Brandon et al., 1999, 2007; Lassiter et al., 2000, 2004; Skovgaard et al., 2001; Eisele et al., 2002; Workmann et al., 2004; Gaffney et al., 2005; Jamais et al., 2008; Debaille et al., 2009; Ireland et al., 2009; Day et al., 2009; Class et al., 2009). Dataset generated using GEOROC and filtered for EM-basalts with [Os] ≥ 40 ppt

1565 to control for the effects of crustal contamination. White bar represents the range of melts
1566 produced by melting only silicate components from a fertile mantle precursor ($^{187}Os/^{188}Os$ =
1567 0.130), [Os] controlled by abundances measured in handpicked silicate aggregates from this
1568 study and their approximate modal abundance). $D_{Os}^{olivine/melt}$ = 0.51 from Burton et al., (2002)
1569 but also modelled for $D_{Os}^{olivine/melt}$ of up to an order of magnitude greater to account for the
1570 full range of PGE $D^{olivine/melt}$ with decreasing oxygen fugacity of Brenan et al. (2003). The Os
1571 elemental abundance and isotope systematics of EM-basalts worldwide can be accounted for
1572 by the sequential addition of first interstitial sulfides (1) followed by a contribution from
1573 formerly enclosed sulfides (2) as melt depletion in the source peridotite continues (see text).
1574 White circles denote individual Kilbourne Hole sulfides (this study), light- and mid-grey
1575 circles are non-cratonic peridotite-derived sulfides from the Mid-Atlantic Ridge and the
1576 French Massif Central (Harvey et al., 2006; 2010 respectively) and black circles are cratonic
1577 sulfides (e.g. Griffin et al., 2004; Aulbach et al., 2004; Marchesi et al., 2009).
1578
1579 Figure 9. Correlation of paired IPGE and paired PPGE in peridotite, individual peridotite-
1580 derived sulfides and basalt. Compositions normalized to CI-chondrite (Horan et al., 2003). (i)
1581 Ir_N vs. Os_N for peridotites from this study (a), worldwide peridotites; inset = this study (b),
1582 mantle derived sulfides (c), and worldwide basalts (d). (ii) Pd_N vs. Pt_N, (iii) Pt_N vs. Os_N. The
1583 strong correlation of pairs of IPGE (i) and pairs of PPGE (ii), but lack of correlation between
1584 IPGE/PPGE pairs (iii) suggests that the two groups behave independently during progressive
1585 melt depletion. Key: (a) Yellow discs = this study (b) Yellow discs = this study; red discs =
1586 Bene Boussera, dark brown discs = Lesotho, grey discs = Namibia, orange discs = Vitim
1587 (Pearson et al., 2004); light blue discs = Oman ophiolite, (Hanghøj et al., 2010); purples discs
1588 = Atlas, Morocco (Wittig et al., 2010); pink discs = Massif Central (Lorand et al., 2003). (c)
1589 Pink discs = Massif Central (Lorand et al., 2003); Dark green discs = Slave Craton, Canada

(Aulbach et al., 2004); White discs = abyddal peridotite (Luguet et al., 2001, 2003, 2004). (d) White discs = Kilauea basalts (Pitcher et al., 2009); dark grey discs = Guizhou, China (Qi & Zhou, 2008); light grey discs = Hawaiian picrite (Ireland et al., 2010); black discs = Phillippines Sea (Dale et al., 2008). For interpretation of the references to colour in this figure legend, the reader is refered to the web version of this article.

1615

1616 # TABLES

Sample	Al_2O_3/SiO_2	[Os]	[Re]	$^{187}Os/^{188}Os$	2 s.e.	$^{187}Re/^{188}Os$	T_{RD}
KH03-10(L)[a]	0.282	0.13	0.40	0.16961	0.00007	0.16963	[b]
KH03-2[c]	0.063	1.39	0.04	0.12125	0.00013	0.12408	0.85
KH03-3[c]	0.096	1.22	0.07	0.13391	0.00014	0.26948	[b]
KH03-4[c]	0.086	2.02	0.07	0.12966	0.00016	0.14829	[b]
KH03-5[c]	0.070	2.10	0.08	0.12723	0.00013	0.17084	[b]
KH03-6[c]	0.072	1.54	0.06	0.12668	0.00017	0.18251	0.05
KH03-6[ce]	-	1.60	0.08	0.12721	0.00026	0.24318	[b]
KH03-6[ce]	-	1.48	0.06	0.12689	0.00010	0.18255	0.02
KH03-6[ce]	-	1.52	0.06	0.12701	0.00016	0.17263	0.00
KH03-7[c]	0.055	2.25	0.07	0.12260	0.00014	0.13757	0.65
KH03-10[c]	0.072	3.36	0.19	0.12520	0.00013	0.26084	0.27
KH03-10[de]	-	3.36	0.19	-	-	-	-
KH03-10[de]	-	3.23	0.23	-	-	-	-
KH03-11[c]	0.078	1.63	0.07	0.12570	0.00018	0.20013	0.19
KH03-12[c]	0.078	1.92	0.10	0.12566	0.00026	0.22697	0.20
KH03-14[c]	0.090	1.52	0.07	0.12911	0.00030	0.22039	[b]
KH03-15[c]	0.027	2.01	0.02	0.12131	0.00016	0.04353	0.84
KH03-15[de]	-	2.01	0.02	-	-	-	-
KH03-15[de]	-	2.04	0.03	-	-	-	-
KH03-16[c]	0.025	2.84	0.01	0.11600	0.00026	0.00872	1.62
KH03-16[de]	-	2.96	0.002	-	-	-	[-]
KH03-16[de]		3.04	0.01	-	-	-	[-]
KH03-17[c]	0.079	1.83	0.07	0.12775	0.00013	0.17599	[b]
KH03-18[c]	0.075	2.50	0.12	0.12627	0.00043	0.2138	0.11
KH03-18[de]	-	2.40	0.16	-	-	-	[-]
KH03-18[de]	-	2.50	0.12	-	-	-	[-]
KH03-21[c]	0.097	1.72	0.13	0.13247	0.00011	0.30562	[b]
KH03-21[ce]	-	1.71	0.07	0.13235	0.00012	0.18475	[b]
KH03-21[ce]	-	1.79	0.06	0.13215	0.00027	0.15138	[b]
KH03-21[de]	-	1.72	0.13	-	-	-	-
KH03-21[de]	-	1.71	0.07	-	-	-	-
KH03-21[de]	-	1.79	0.06	-	-	-	-
KH03-21[de]	-	1.73	0.08	-	-	-	-
KH03-22[c]	0.057	1.75	0.05	0.12137	0.00030	0.13257	0.83
KH03-23[c]	0.076	1.59	0.07	0.12488	0.00011	0.19362	0.32
KH03-24[c]	0.059	1.39	0.06	0.12334	0.00014	0.14757	0.54
KH03-24[ce]	-	1.79	0.04	0.11919	0.00020	0.07685	1.16
KH03-24[de]	-	1.39	0.06	-	-	-	-
KH03-24[de]	-	1.39	0.05	-	-	-	-
KH03-25[c]	0.050	1.73	0.02	0.11936	0.00015	0.05207	1.13
KH03-26[c]	0.078	1.44	0.05	0.12687	0.00012	0.16681	0.02
KH03-27[c]	0.030	1.54	0.03	0.12031	0.00356	0.08833	0.99

KH96-1[c]	0.065	1.18	0.05	0.12411	0.00030	0.05244	0.43
KH96-2[c]	0.041	1.16	0.03	0.11885	0.00013	0.12372	1.21
KH96-8[c]	0.063	1.60	0.28	0.13090	0.00013	0.83201	[b]
KH96-18[c]	0.075	0.80	0.04	0.12936	0.00014	0.19627	[b]
KH96-20[c]	0.082	2.26	0.27	0.13268	0.00014	0.4895	[b]
KH96-21[c]	0.019	3.54	0.02	0.11588	0.00014	0.02138	1.64
KH96-24[c]	0.059	2.39	0.68	0.12679	0.00014	1.35525	0.03

Table 1. Bulk-rock Al_2O_3/SiO_2, Re and Os elemental abundance and Re-Os isotope systematics of 28 peridotite xenoliths from Kilbourne Hole, New Mexico, USA. Al_2O_3/ SiO_2 calculated from wt.% of oxides derived by XRF at The Open University. Major element data quality assessed using two rock standards (WS-E and OUG-94). Reproducibility is within 2% of recommended values. Complete major and trace element abundances for all of the samples are the subject of a separate contribution (Hammond et al., 2010). [Re] and [Os] expressed in parts per billion (ppb). Errors shown as 2σ mean. T_{RD} = (minimum) time of rhenium depletion calculated using a mean present-day chondritic value$^{187}Os/^{188}Os = 0.127$ (Luck & Allègre, 1983; Walker & Morgan, 1989) and assumes that $^{187}Re/^{188}Os_{sample} = 0$. Given isotope ratios blank corrected. $^{187}Os/^{188}Os$ ratios normalised to $^{192}Os/^{188}Os = 3.08271$ and corrected using measured $^{18}O/^{16}O$ and $^{17}O/^{16}O$ of 0.002047 and 0.00037, respectively. Johnson Matthey (n = 26) 2.75 ng Os standard $^{187}Os/^{188}Os = 0.17373 \pm 12$ (2σ). [a] host lava. [b] "future" age. [c] Carius tube digestion. [d] high pressure asher digestion for PGE concentration measurement. For all PGE abundances please refer to Table 4. [e] duplicate measurement.

Sample	[Os]	[Re]	$^{187}Os/^{188}Os$	2 s.e.	$^{187}Re/^{188}Os$
KH03-15 olivine	36.0	24.4	0.1232	0.0007	5.11
KH03-15 opx	45.9	36.8	0.1315	0.0018	6.08
KH03-15 cpx	420	37.4	0.1250	0.0009	0.68
KH03-15 spinel	1633	47.1	0.1215	0.0005	0.22
KH03-16 olivine	10.4	22.0	0.1238	0.0022	10.0
KH03-16 opx	142	53.4	0.1201	0.0008	0.26
KH03-16 cpx	2620	535.8	0.1167	0.0003	0.97
KH03-16 spinel	805	520.2	0.1307	0.0017	3.35
KH03-21 olivine	33.6	2.84	0.1309	0.0006	0.63
KH03-21 opx	38.2	152	0.1328	0.0011	30.1
KH03-21 cpx	63.8	85.7	0.1391	0.0016	10.2
KH03-21 spinel	1630	167	0.1525	0.002	0.78
KH03-24 olivine	26.9	12.2	0.1299	0.0014	3.62
KH03-24 opx	33.7	10.4	0.1324	0.0009	2.35
KH03-24 cpx	65.1	89.1	0.1617	0.0003	10.4
KH03-24 spinel	826	818	0.1245	0.0007	7.51

Table 2. Re–Os isotope data for mineral separates from KH03-15, KH03-16, KH03-21 & KH03-24. Errors shown are 2σ mean. Re and Os concentrations expressed as parts per trillion (ppt). Standards and corrections for $^{18}O/^{16}O$ and $^{17}O/^{16}O$ as in Table 1.

1652

1653

1654

Sample	Ni	Cu	S	Fe	Co	Zn	Si	Total
KH03-11_A1	16.03	0.61	36.69	45.34	0.31	0.00	0.03	99.00
KH03-11_A1	34.14	1.31	33.20	31.15	0.46	0.00	0.01	100.27
KH03-14_A10	16.02	0.78	37.48	44.28	0.31	0.00	0.00	98.87
KH03-14_A10	8.89	4.44	37.16	48.88	0.23	0.00	0.00	99.61
KH03-14_A10	1.74	20.99	34.81	40.17	0.14	0.02	0.00	97.86
KH03-14_A9	15.03	0.63	37.35	45.50	0.31	0.00	0.00	98.83
KH03-14_A8	17.71	0.44	36.37	43.70	0.28	0.00	0.00	98.50
KH03-14_A8	11.40	11.69	35.25	39.97	0.19	0.01	0.00	98.51
KH03-14_A9	1.92	21.44	35.15	39.75	0.13	0.01	0.00	98.40
KH03-14_A7	19.50	4.56	35.08	35.84	0.36	0.02	1.15	96.50
KH03-14_A7	16.13	0.66	37.49	44.63	0.30	0.00	0.00	99.21
KH03-14_A6	13.30	0.44	37.24	47.52	0.26	0.00	0.00	98.76
KH03-14_A5	17.05	0.77	37.19	44.18	0.29	0.00	0.00	99.48
KH03-14_A4	15.76	0.73	37.50	45.33	0.30	0.00	0.00	99.63
KH03-14_A3	14.78	0.37	38.08	45.09	0.30	0.00	0.01	98.63
KH03-14_A2	14.66	0.55	37.64	45.99	0.31	0.01	0.00	99.16
KH03-14_A1	15.14	0.77	37.31	45.98	0.31	0.00	0.00	99.52
KH03-15_1.1	28.76	0.68	34.71	35.01	0.30	0.00	0.00	99.47
KH03-17_A1	23.26	0.23	37.93	38.17	0.29	0.00	0.00	99.87
KH03-17_A2	25.88	0.31	37.75	35.64	0.29	0.01	0.00	99.87
KH03-21_1.1	29.39	1.72	32.61	35.26	0.29	0.00	0.00	99.27
KH03-21_1.1	27.32	4.68	32.79	33.87	0.30	0.00	0.00	98.96
KH03-21_1.2	28.45	1.71	33.15	36.13	0.29	0.00	0.00	99.74
KH03-21_1.2	26.90	4.61	33.12	35.02	0.30	0.00	0.00	99.95
KH03-21_1.3	31.95	1.84	32.41	31.81	0.33	0.00	0.00	98.34
KH03-21_1.3	8.79	0.12	37.50	51.19	0.17	0.00	0.00	97.78
KH03-21_2.1	16.27	0.28	37.32	45.54	0.32	0.01	0.00	99.74
KH03-21_2.2	23.86	0.20	37.12	38.23	0.28	0.02	0.00	99.71
KH03-21_2.2	2.69	22.59	34.17	38.63	0.09	0.00	0.00	98.17
KH03-21_3.1	16.26	0.51	36.61	44.66	0.32	0.00	0.00	98.36
KH03-21_3.2	28.27	2.23	32.06	34.91	0.30	0.00	0.08	97.85
KH03-21_3.2	21.26	9.25	32.34	35.15	0.24	0.00	0.00	98.24

KH03-21_4.1	10.86	0.53	36.61	51.03	0.29	0.00	0.02	99.34
KH03-21_4.1	28.43	0.32	33.99	37.41	0.63	0.00	0.00	100.77
KH03-22_A1	34.08	1.64	33.00	30.58	0.25	0.00	0.02	99.56
KH03-22_A3	17.17	0.62	37.28	44.37	0.27	0.00	0.00	99.71
KH03-22_A3	33.46	1.65	33.16	31.20	0.29	0.00	0.02	99.79
KH03-22_A3	29.88	4.26	34.10	32.16	0.28	0.00	0.00	100.68
KH03-22_A4	34.77	1.21	32.31	30.09	0.28	0.00	0.20	98.85
KH03-22_A4	17.75	0.39	37.76	43.64	0.28	0.00	0.00	99.81
KH03-22_A5	19.17	0.45	37.84	41.91	0.24	0.00	0.00	99.62
KH03-22_A5	36.16	0.95	33.10	28.58	0.29	0.00	0.09	99.17
KH03-22_A6	18.69	0.49	37.39	42.94	0.24	0.00	0.00	99.75
KH03-22_B1.1	14.38	0.32	37.28	45.47	0.20	0.00	0.00	97.65
KH03-22_B1.2	28.23	0.47	34.70	36.35	0.30	0.00	0.03	100.07
KH03-22_B1.3	16.13	0.30	38.29	44.18	0.25	0.00	0.06	99.22
KH03-22_B1.4	31.54	2.12	33.18	30.75	0.32	0.00	0.19	98.09
KH03-22_B1.4	12.55	0.41	38.17	48.15	0.23	0.02	0.03	99.57
KH03-22_B2	19.65	0.54	36.18	40.99	0.24	0.01	0.01	97.63
KH03-22_B3.1	31.93	1.59	33.02	31.86	0.32	0.00	0.02	98.74
KH03-22_B3.1	13.09	0.55	37.36	47.66	0.22	0.00	0.00	98.89
KH03-22_B3.2	34.07	1.11	32.71	30.02	0.30	0.00	0.00	98.21
KH03-22_B3.2	17.56	0.23	37.25	43.34	0.24	0.00	0.00	98.62
KH03-22_B4.2	16.95	0.46	36.98	43.82	0.27	0.01	0.07	98.57
KH03-22_B4.1	32.71	1.00	33.49	30.94	0.29	0.00	0.00	98.42
KH03-22_B4.1	19.94	0.56	37.44	40.68	0.28	0.00	0.00	98.91
KH03-23_A1	1.10	25.91	34.21	36.11	0.04	0.01	0.01	97.39

Table 3. Major element abundances of sulfide grains in peridotite xenoliths from Kilbourne Hole, New Mexico, USA. Repeat analyses of an in-house pentlandite standard yields errors on major elements (S, Fe, Ni) of 2, 5 and 6 % (2 σ) respectively, with minor elements (Co, Cu) errors (2 σ) of 22% and 70% respectively.

Sample	[Os]	2sd	[Ir]	+/-	[Ru]	+/-	[Pt]	+/-	[Pd]	+/-	[Re]	2sd
KH03-10(L)[a]	0.13	0.01	0.14	0.01	0.31	0.02	0.48	0.19	0.61	0.24	0.40	0.16
KH03-10	3.36		4.19	0.25	7.47	0.45	6.58	2.63	5.58	2.23	0.19	
KH03-10[b]	3.23										0.26	
mean	*3.30*	*0.18*									*0.23*	*0.11*
KH03-15	2.01		3.07	0.18	5.43	0.33	4.31	1.73	1.26	0.50	0.02	
KH03-15[b]	2.04										0.03	
mean	*2.02*	*0.04*									*0.02*	*0.01*
KH03-16	2.84		3.04	0.18	4.77	0.29	3.35	1.34	0.55	0.22	0.007	
KH03-16[b]	2.96										0.002	
mean	*2.90*	*0.18*									*0.004*	*0.008*
KH03-18	2.50		3.44	0.21	6.21	0.37	6.12	2.45	4.55	1.82	0.12	
KH03-18[b]	2.40										0.16	
mean	*2.45*	*0.14*									*0.14*	*0.06*
KH03-21	1.72		2.81	0.17	5.25	0.31	4.56	1.82	2.74	1.10	0.13	
KH03-21[b]	1.71										0.07	
KH03-21[b]	1.79										0.06	
KH03-21[b]	1.73										0.08	
mean	*1.74*	*0.09*									*0.08*	*0.03*
KH03-24	1.39		2.84	0.00	5.14	0.00	4.66	1.86	2.59	1.04	0.06	
KH03-24[b]	1.39										0.05	
mean	*1.39*	*0.00*									*0.05*	*0.02*

Table 4. Platinum group element (+ Re) abundances in bulk-rock Kilbourne Hole peridotite xenoliths and host basalt. All concentrations shown in parts per billion (ppb). Precision of [Ir] & [Ru] measurements (± 6%) calculated from the external reproducibility of [Os] on multiple measurements on several powder splits from each xenolith. Precision of [Pd] & [Pt] (± 40%) calculated from the external reproducibility of [Re]. Internal, i.e. within-run precision is more than an order of magnitude better than external precision which is therefore the limiting factor on PGE concentration reproducibility in these samples. [a] host lava. [b] duplicate measurement by Carius tube digestion (or some HPA?).

Sample	Morphology	[Os]	[Re]	$^{187}Os/^{188}Os$	2 s.e.	$^{187}Re/^{188}Os$
KH03-15_2	interstitial	0.001	0.848	0.2163	0.0073	3575
KH03-15_4	enclosed	24.70	11.3	0.1195	0.0003	2.18
KH03-15_5	enclosed	36.9	2.83	0.1208	0.0002	0.37
KH03-15_6	enclosed	10.9	0.140	0.1202	0.0002	0.03
KH03-15_7	interstitial	6.05	-	0.1304	0.0003	-
KH03-15_9	enclosed	5.82	-	0.1185	0.0003	-
KH03-15_10	interstitial	21.2	-	0.1312	0.0004	-
KH03-16_2	interstitial	0.51	1.35	0.1349	0.0015	12.7
KH03-16_3	interstitial	0.010	138.9	0.1424	0.0050	68722
KH03-16_4	interstitial	1.48	34.27	0.1556	0.0051	111
KH03-16_5	enclosed	12.9	0.294	0.1235	0.0001	0.11
KH03-16_6	interstitial	0.024	3.133	0.1819	0.0057	622
KH03-16_9	interstitial	1.74	-	0.1362	0.0010	-
KH03-16_10	interstitial	0.052	-	0.3729	0.0169	-
KH03-21_1	interstitial	0.992	1.252	0.1303	0.0006	6.02
KH03-21_2	interstitial	1.11	1.181	0.1694	0.0004	5.11
KH03-21_3	enclosed	2.72	0.056	0.1283	0.0003	0.098
KH03-21_4	interstitial	10.0	23.32	0.1291	0.0001	101
KH03-21_5	enclosed	9.97	-	0.1259	0.0008	-
KH03-21_6	interstitial	1.29	-	0.1302	0.0008	-
KH03-21_7	interstitial	0.843	-	0.1368	0.0008	-
KH03-21_8	enclosed	4.48	-	0.1282	0.0005	-
KH03-21_9	interstitial	0.447	-	0.1764	0.0012	-
KH03-21_10	interstitial	0.584	-	0.1385	0.0005	-
KH03-24_5	enclosed	1.69	0.01	0.1227	0.0004	0.020
KH03-24_10	enclosed	0.195	0.002	0.1237	0.0028	0.050
KH03-24_11	enclosed	0.231	-	0.1240	0.0006	-
KH03-24_14	enclosed	2.76	0.04	0.1226	0.0013	0.070
KH03-24_15	enclosed	2.54	35.87	0.1234	0.0004	67.4
KH03-24_16	enclosed	2.50	18.78	0.1238	0.0011	35.8
KH03-24_17	interstitial	0.600	27.27	0.1264	0.0005	217
KH03-24_20	interstitial	0.314	-	0.1449	0.0017	-

Table 5. Re–Os elemental abundance and isotope data for sulfides from KH03-15, KH03-16, KH03-21 and KH03-24. Errors shown are 2 σ mean. Re and Os concentrations expressed as parts per million (ppm). Standards and corrections for $^{18}O/^{16}O$ and $^{17}O/^{16}O$ as in Table 2.

FIGURES

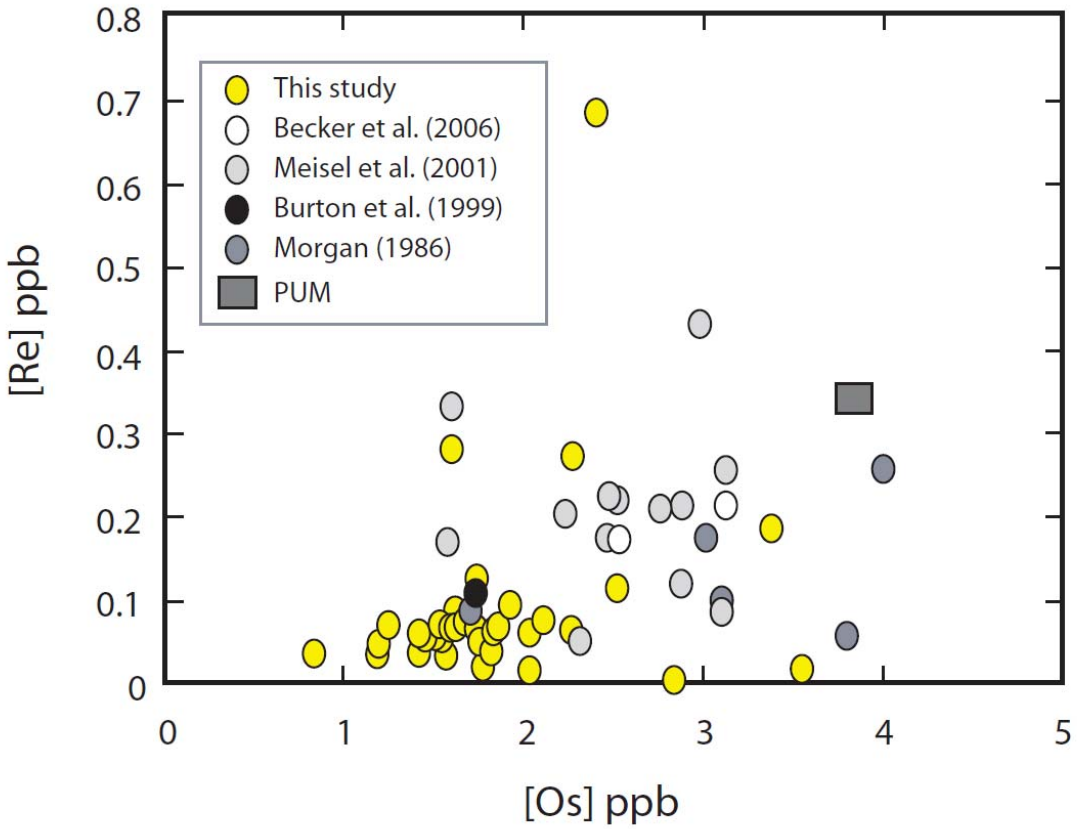

Figure 1

1726

1727

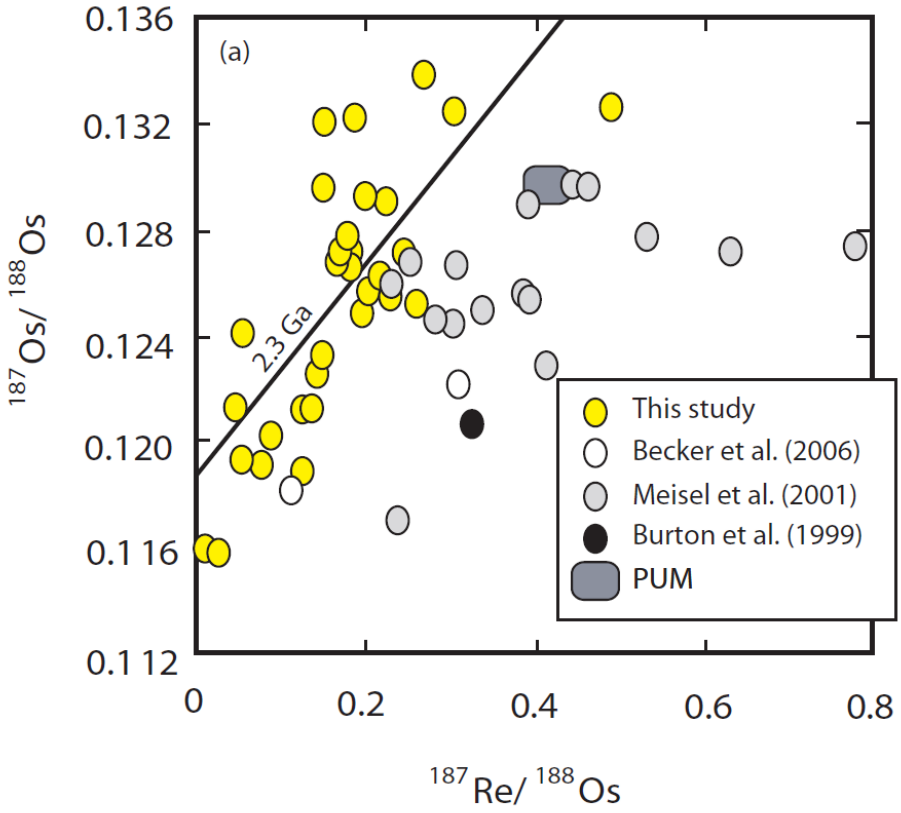

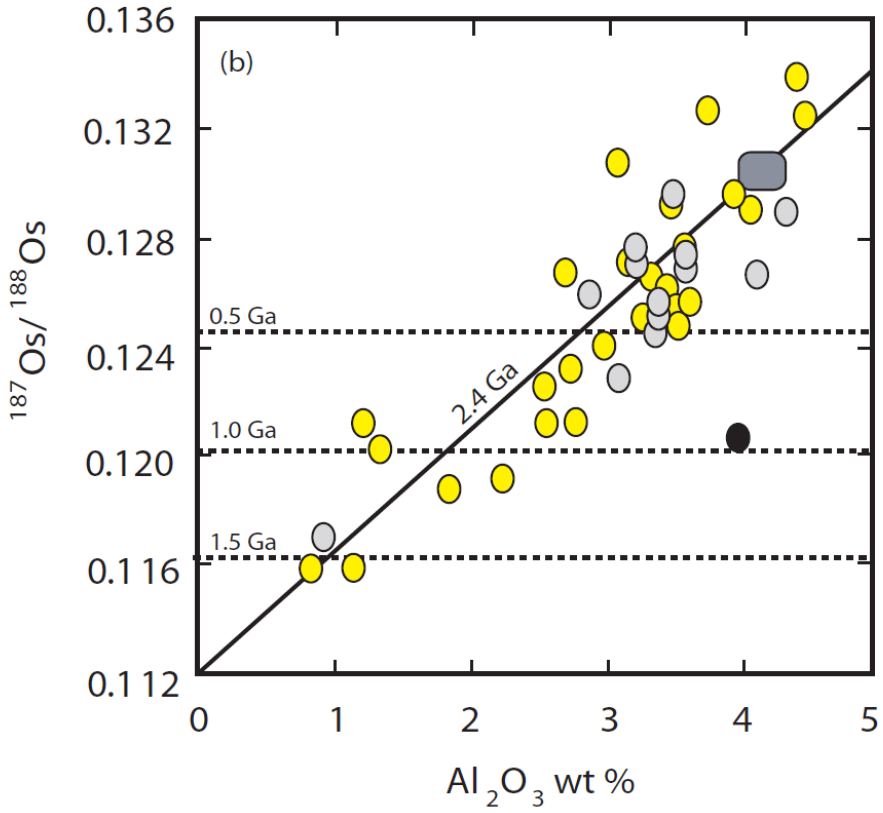

1728

1729 Figure 2

1730

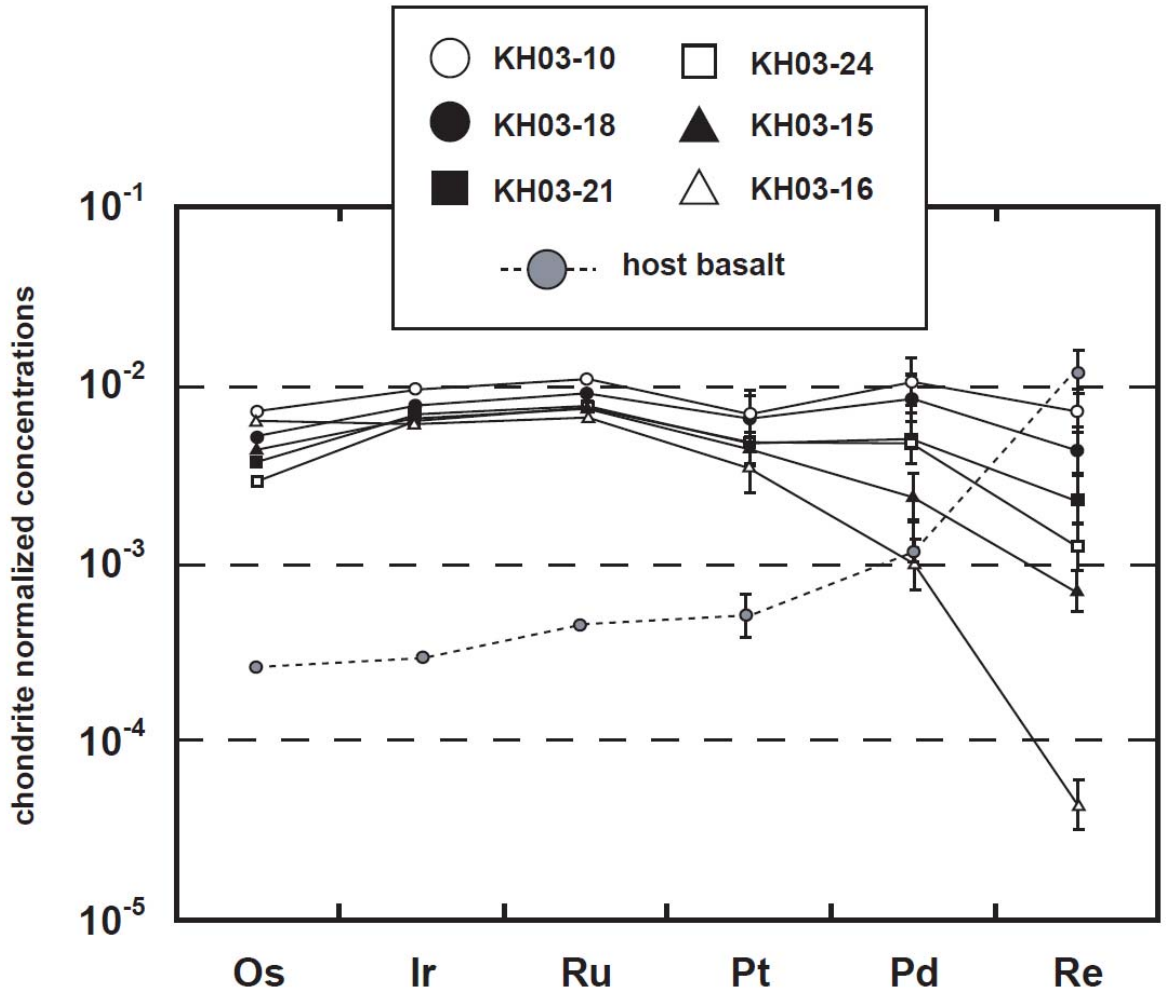

1731

1732 Figure 3

1733

1734

1735

1736

1737

1738

1739

1740

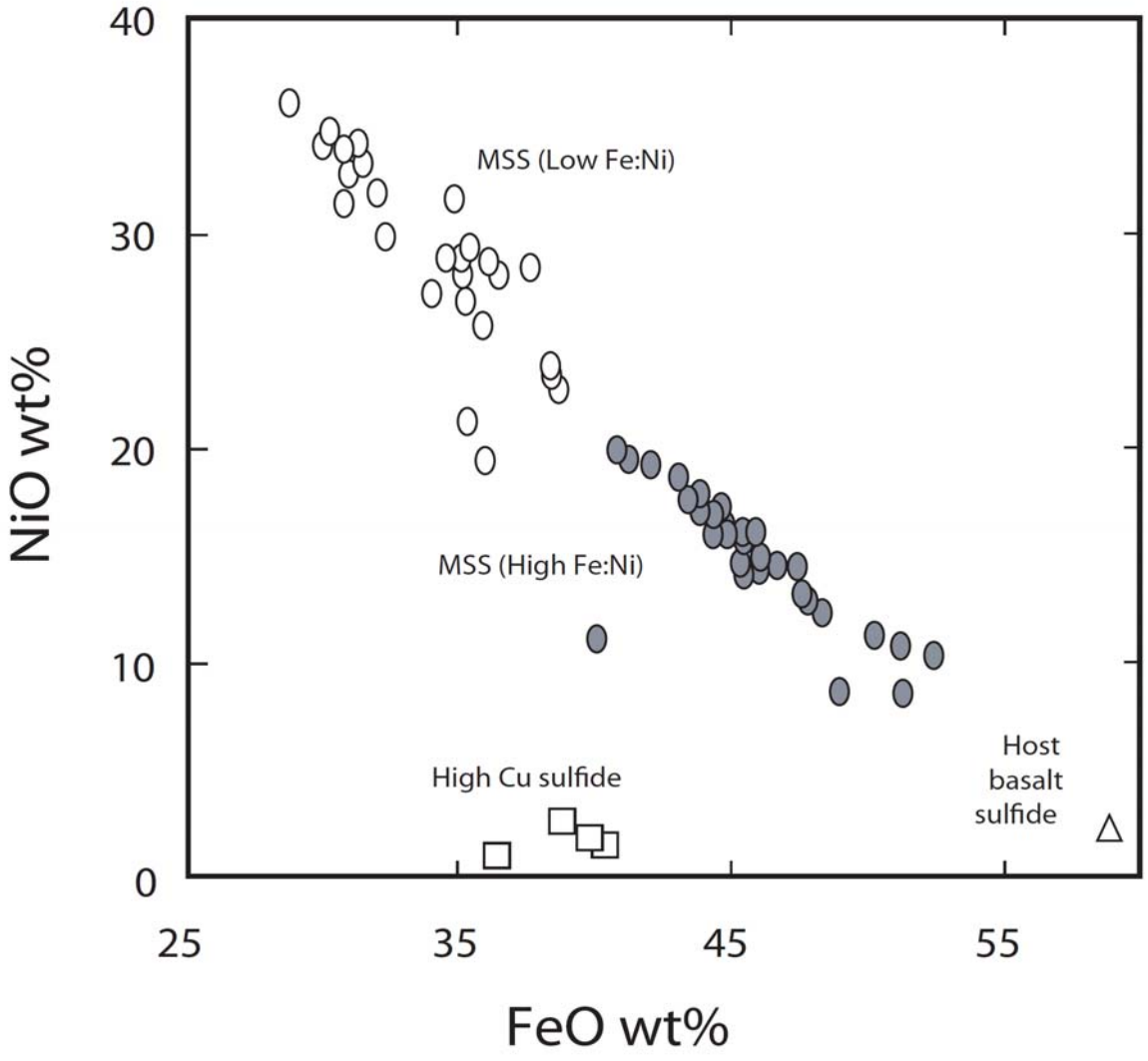
40
30
20
10
0
NiO wt%
MSS (Low Fe:Ni)
MSS (High Fe:Ni)
High Cu sulfide
Host
basalt
sulfide
25
35
45
55
FeO wt%

Figure 4

1752

1753

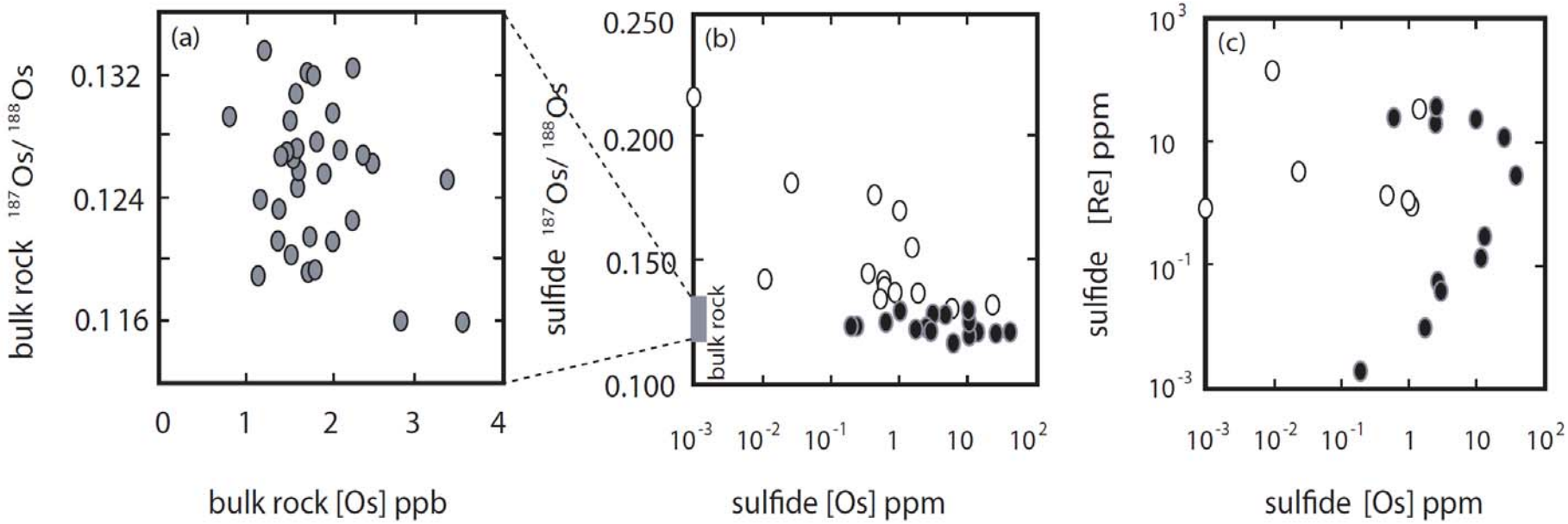

1754

1755 Figure 5

1756

1757

1758

1759

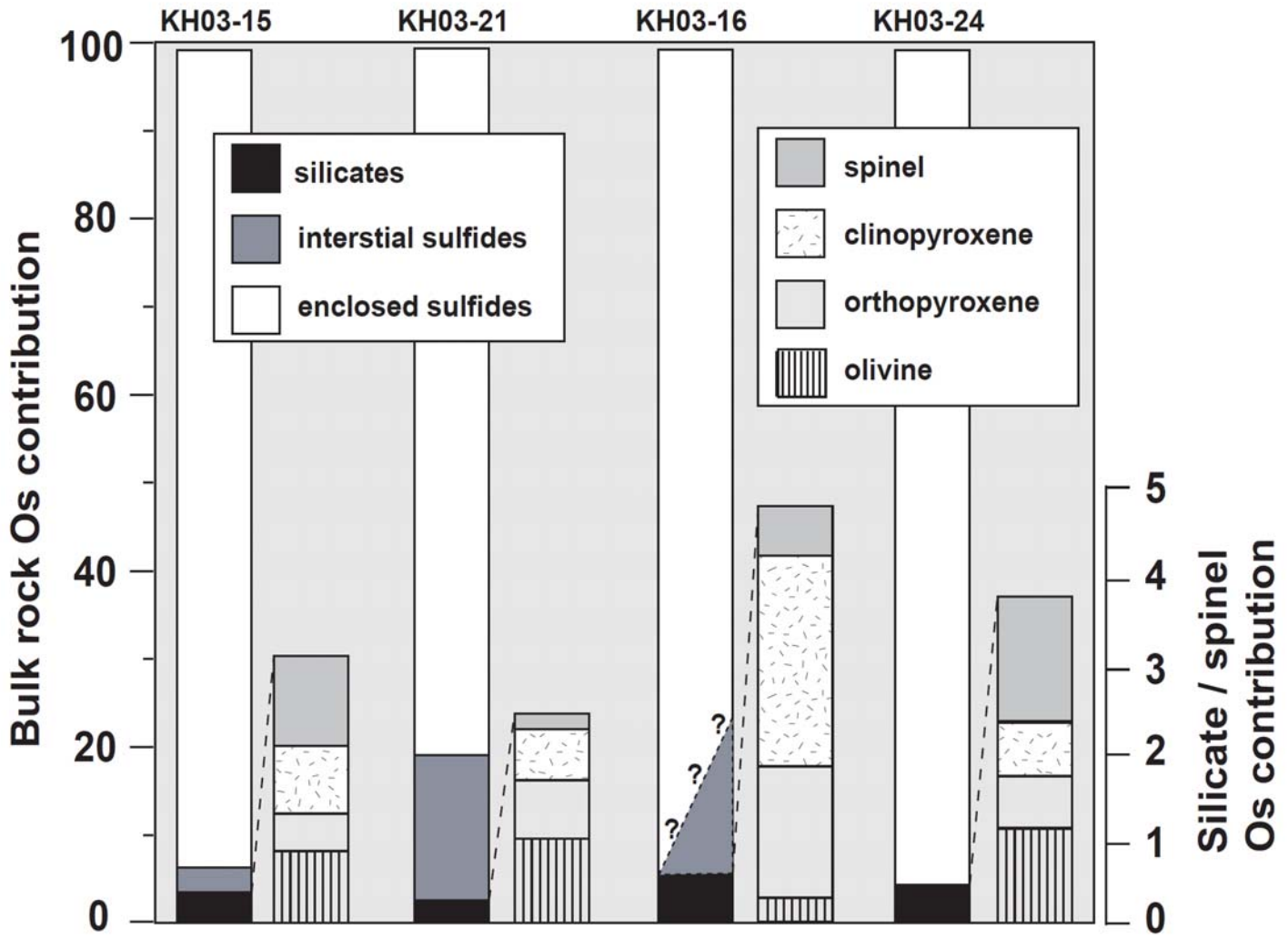

1760

1761 Figure 6

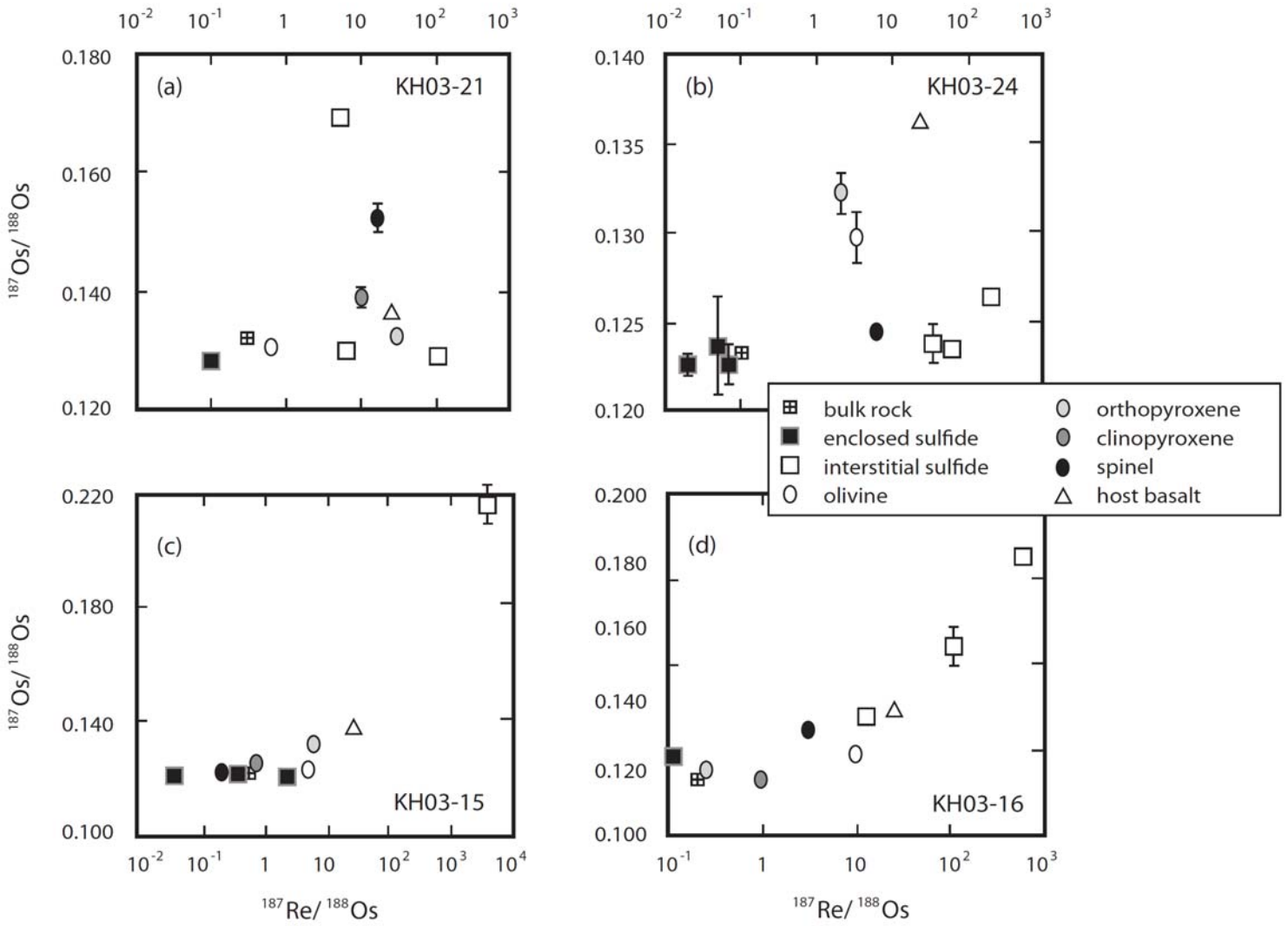

1762

1763 Figure 7

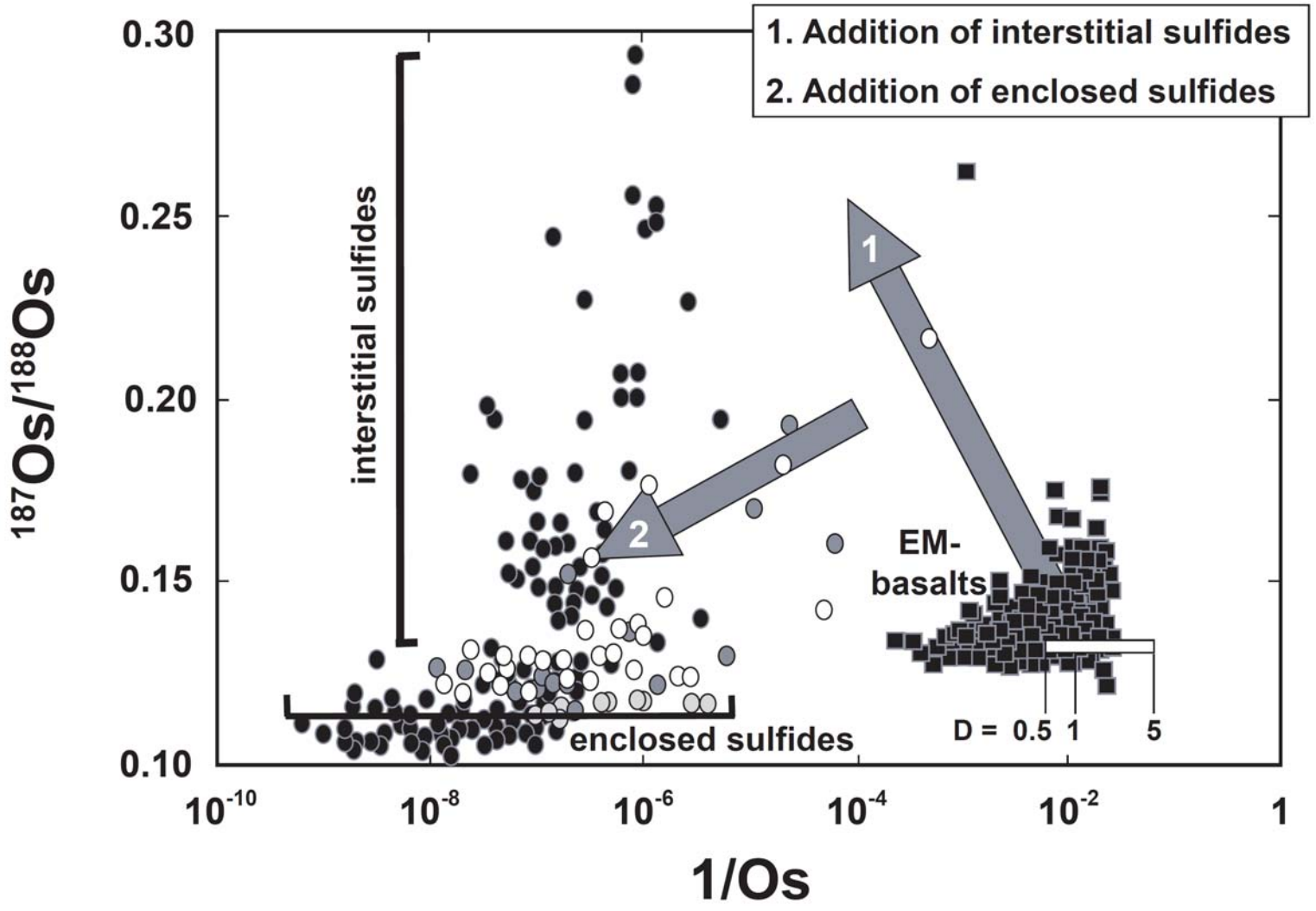

1764

1765 Figure 8

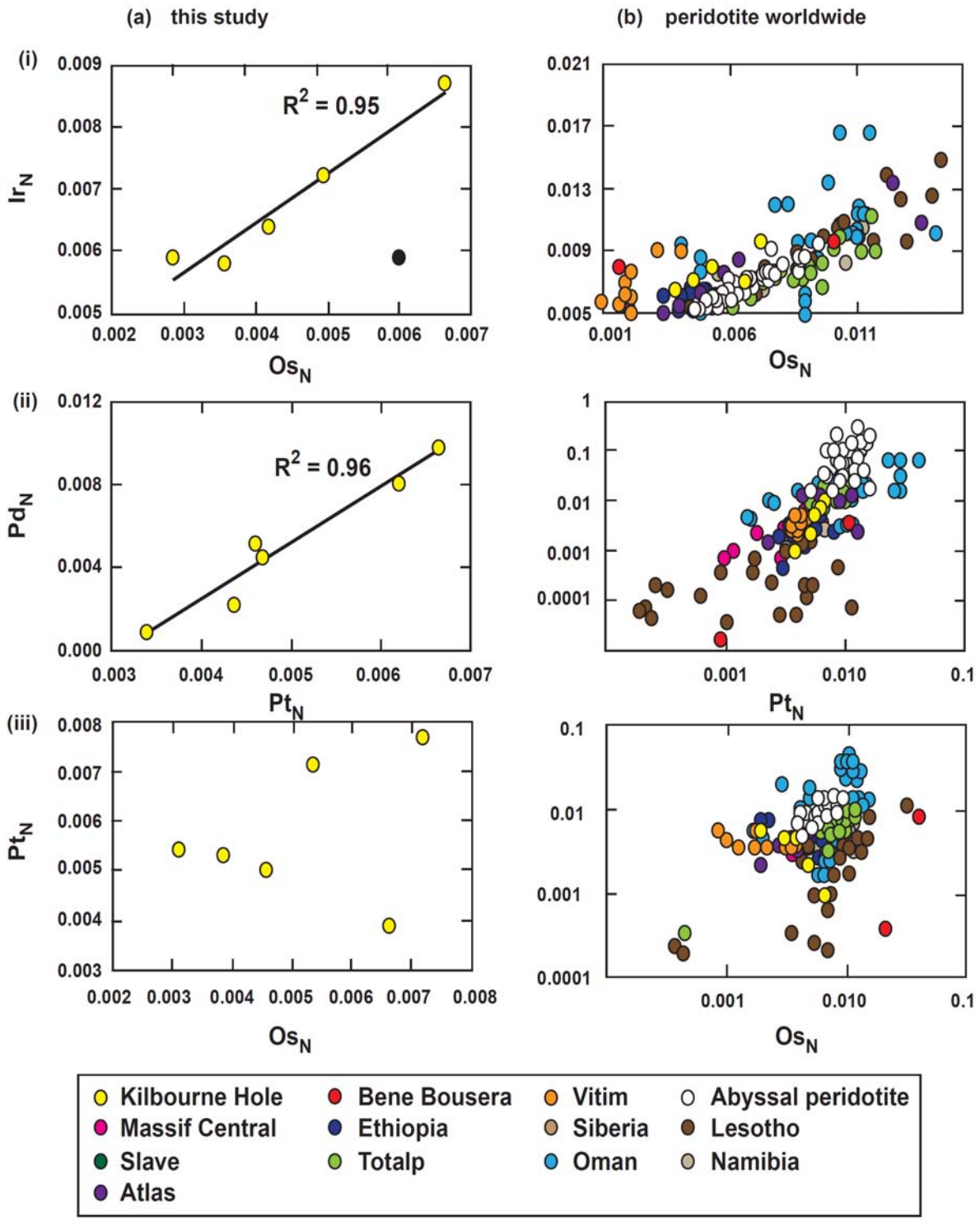
(a) this study
(b) peridotite worldwide
(i)
(ii)
(iii)
R2 = 0.95
R2 = 0.96
IrN
PdN
PtN
OsN
Kilbourne Hole
Massif Central
Slave
Atlas
Bene Bousera
Ethiopia
Totalp
Vitim
Siberia
Oman
Abyssal peridotite
Lesotho
Namibia

Figure 9 a

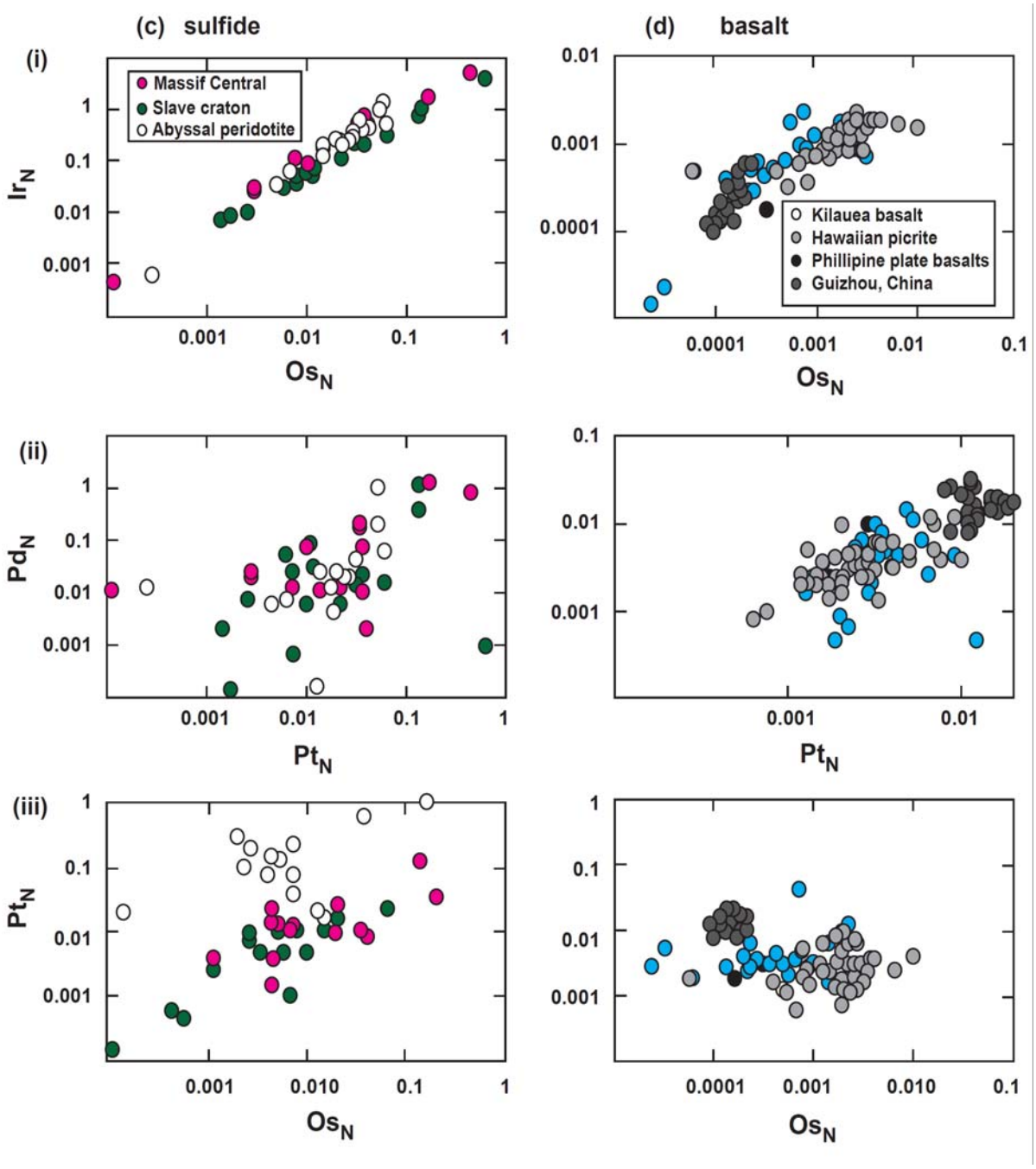

1771

1772 Figure 9 c & d